T H E U N I V E R S I T Y O F M I C H I G A N

COLLEGE OF ENGINEERING
Department of Engineering Mechanics

Technical Report

THE CYLINDRICAL SHELL OF FINITE LENGTH UNDER A NEARLY UNIFORM RADIAL IMPULSE

ORA Project 08371

supported by:

NATIONAL SCIENCE FOUNDATION
GRANT NO. GK-1251
WASHINGTON, D.C.

administered through:

OFFICE OF RESEARCH ADMINISTRATION ANN ARBOR

June 1967

This report was also a dissertation submitted by the first author in partial fulfillment of the requirements for the degree of Doctor of Philosophy in The University of Michigan, 1967.

ACKNOWLEDGMENTS

I would like to thank the committee members for their assistance, time, and interest. I am particularly indebted to Professor Ivor K. McIvor, the committee chairman, for his excellent and generous guidance throughout the course of this research.

The financial assistance of the Ford Foundation and the National Science Foundation is gratefully acknowledged.

Throughout my graduate studies and especially during the terminal stages of the research, my wife Ellen has been exceptionally patient and understanding. I am very grateful to her.

TABLE OF CONTENTS

LIST OF FIGURES

LIST OF FIGURES (Concluded)

NOMENCLATURE

$A_1, A_2, \ldots, A_9$	Constants of integration
$C_1, C_2, \ldots, C_{13}$	Combinations of a, h, ℓ, m, and n
E	Modulus of elasticity
F_1, F_2, F_3	Circular frequencies
$\tilde{F}$	Circular frequency for first linear approximation
$\approx{F}$	Circular frequency for second linear approximation
U_{mn}, V_{mn}, W_{mn}	Coefficients in the Fourier expansions of u, v, and w
a	Radius of the shell's midsurface
c	Wave velocity, $[E/\rho(1-\nu^2)]^{1/2}$
h	Thickness of the shell
i, j	Integers
k	Growth parameter for unstable solutions
ℓ	Length of the shell
m, n	Integers
t	Time
u, v, w	Axial, circumferential and radial displacements
v_o	Uniform radial velocity initially imparted to the shell
x, θ, z	Cylindrical coordinates
Δ	Small number
Ω, μ	Parameters of the Mathieu equation
ϵ_{mn}	Small number in the velocity perturbation

$\epsilon_x, \epsilon_\theta, \epsilon_z$	Normal strains
$\epsilon_{x\theta}, \epsilon_{\theta z}, \epsilon_{zx}$	Shear strains
$\kappa_x, \kappa_\theta, \kappa_{x\theta}$	Coefficients of z in the strain expressions
$\mu_\theta, \mu_{x\theta}$	Coefficients of z^2 in the strain expressions
ν	Possion's ratio
ρ	Material density
σ_x, σ_θ	Axial and circumferential normal stress
$\sigma_x^*, \sigma_\theta^*$	Maximum values of axial and circumferential stress
τ	Dimensionless time, ct/a
$(\dot{})$	Dimensionless time derivative, $d(\ )/d\tau$
$(\bar{})$	Midsurface quantity

ABSTRACT

The shell considered is thin-walled, having a circular cross section and an arbitrary length. Boundary supports permit radial and circumferential displacements while requiring the slope in the longitudinal direction and the axial displacement to vanish at the ends. The material is linear and elastic. Under a uniform radial impulsive loading, this shell responds with simple harmonic radial motion, independent of circumferential and axial location. The principal issue of the investigation is the stability of this motion.

The strain measures are nonlinear functions of midsurface displacements and displacement gradients. The longitudinal, circumferential and radial displacements are taken as double Fourier series satisfying the boundary conditions. Lagrange equations are developed for the time-dependent coefficients of the series after the energy has been expressed in terms of them. The result is an infinite set of second order, coupled, nonlinear differential equations. The initial conditions consist of the uniform radial impulse with a superimposed spatial perturbation.

The equations of the nonlinear problem may be uncoupled by neglecting tangential inertia. To evaluate the quality of this approximation, a study is made of the linear problem. The exact linear solutions are compared with the approximate linear solutions. The agreement is excellent for purely radial loading.

For the initial behavior, the perturbation-dependent flexural terms appearing in the breathing mode equation may be neglected. By retaining only nonlinear terms which are products of fundamental and flexural coefficients in the differential equations for the flexural coefficients, the results is a set of Mathieu equations. The excitation of particular "unstable" modes is determined from an evaluation of an equation's parameters. These are functions of both the shell geometry and the initial perturbational velocities.

For a study of long-time behavior, consideration is given only to the breathing mode and those flexural modes whose excitation is predicted by the short-term analysis. The resulting nonlinear differential equations are integrated numerically. The response is characterized by a cyclic energy exchange between the various modes. Generally the long-term behavior is dominated by a few flexural modes having the highest growth rates.

If flexural motion is excited, it gives rise to stresses that are far in excess of those associated with the basic motion of the shell.

CHAPTER I

INTRODUCTION

The response of a thin-walled elastic cylindrical shell of finite length to a uniform radial impulse is a simple harmonic motion in which the cross section remains circular, periodically expanding and contracting. The longitudinal variation of the radial displacement depends upon the boundary conditions; the amplitude depends upon the particular shell geometry, material properties, and the intensity of the loading. The stability of this motion is the central issue in this investigation.

The given motion is unstable if in the presence of small irregularities in the initial loading, the subsequent motion deviates significantly from the unperturbed response. Such deviations may occur because of the nonlinear coupling between the modes of oscillation. A number of predominantly flexural modes can be parametrically excited to rather large amplitudes. Energy is extracted from the initial or basic response and cyclically exchanged between the modes exhibiting significant growth.

In Chapter II a nonlinear formulation of the shell problem is derived. The analysis of the nonlinear problem can be simplified considerably by neglecting tangential inertia in the equations of motion. The appropriateness of this approximation is ascertained by studying the linear vibrations of the shell in Chapter III.

A criterion for the stability of the basic response is obtained in Chapter IV, and its dependence upon the shell geometry is established. In

addition, those flexural modes which may exhibit significant growth are identified. With the critical modes determined, the nonlinear equations for a given problem can be integrated numerically to obtain the finite time response of the shell. In the present study a number of specific examples are considered. The displacements and stresses are much larger than those associated with the unperturbed motion. Finally the examples serve to delineate the perturbation sensitivity of the response.

In related problems, Bolotin[1]* presented a formulation for the dynamic stability of the thin cylindrical shell. Unlike the present investigation in which the source of excitation is internal, i.e., pulsating membrane forces, in Bolotin's case the excitation source was external. The particular loadings considered by Bolotin were axial compression and radial pressure, both simple harmonic functions of time.

Goodier and McIvor[2] have analyzed the cylindrical shell loaded by a nearly uniform radial impulse. The investigation was restricted to the case of plane strain, i.e., requiring generators of the shell to remain straight and parallel to the axis. The analysis that follows in this thesis considers displacement variations along the length of the cylinder.

The simply supported cylindrical shell subjected to a suddenly applied pressure has been considered by Bieniek, Fan, and Lackman[3] using Galerkin's method. From a short term analysis, the growth of displacement perturbations is predicted. The influence of length upon the short term response is not discussed nor is the long term motion analyzed.

*A raised number is a Bibliographical entry.

CHAPTER II

FORMULATION OF THE PROBLEM

A. STRAIN-DISPLACEMENT RELATIONS

The cylindrical shell considered is shown in Fig. 1. The constants denoting the length, thickness, and midsurface radius are ℓ, h, and a, respectively. With the origin at one end of the midsurface, the coordinates in the longitudinal, circumferential, and radial directions are x, θ and z, and the corresponding displacement components of a generic point are u, v, and w.

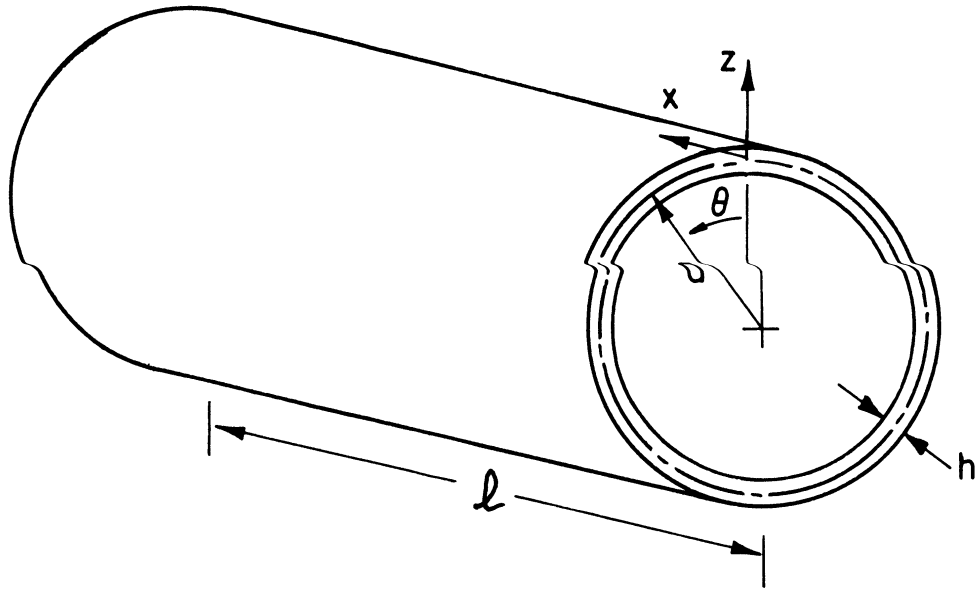

Fig. 1. Shell geometry and coordinate system.

To develop a nonlinear shell theory appropriate for the ensuing stability analysis, it is necessary to retain quadratic terms in the strain-displacement relations. But in the motion of thin shells, the tangential components of the displacement are generally small compared to the radial component. Thus quadratic terms involving only w and its derivatives are retained. With

this, the strain components at a typical point are

$$\epsilon_x = \frac{\partial u}{\partial x} + \frac{1}{2}\left(\frac{\partial w}{\partial x}\right)^2 \tag{2.1}$$

$$\epsilon_\theta = \frac{1}{(a+z)}\left(w + \frac{\partial v}{\partial \theta}\right) + \frac{1}{2(a+z)^2}\left[w^2 + \left(\frac{\partial w}{\partial \theta}\right)^2\right] \tag{2.2}$$

$$\epsilon_z = \frac{\partial w}{\partial z} + \frac{1}{2}\left(\frac{\partial w}{\partial z}\right)^2 \tag{2.3}$$

$$\epsilon_{x\theta} = \frac{\partial v}{\partial x} + \frac{1}{(a+z)}\left(\frac{\partial u}{\partial \theta}\right) + \frac{1}{(a+z)}\left(\frac{\partial w}{\partial x}\right)\left(\frac{\partial w}{\partial \theta}\right) \tag{2.4}$$

$$\epsilon_{\theta z} = \frac{\partial v}{\partial z} + \frac{1}{(a+z)}\left[\frac{\partial w}{\partial \theta} - v + \frac{\partial w}{\partial \theta}\frac{\partial w}{\partial z}\right] \tag{2.5}$$

$$\epsilon_{zx} = \frac{\partial u}{\partial z} + \frac{\partial w}{\partial x} + \frac{\partial w}{\partial x}\frac{\partial w}{\partial z} \tag{2.6}$$

In the work that follows, a bar over a quantity will denote its midsurface value. For thin shells the functional dependence of the displacements upon the thickness coordinate may be prescribed by introducing the Kirchhoff-Love approximation. Essentially this requires that the strains ϵ_z, $\epsilon_{\theta z}$, and ϵ_{zx} vanish. Setting the normal strain ϵ_z equal to zero gives

$$w = w(x,\theta) = \bar{w} \tag{2.7a}$$

Setting $\epsilon_{\theta z}$ equal to zero and making use of (2.7a) gives

$$\frac{v}{(a+z)} = \frac{\partial \bar{w}}{\partial \theta}\frac{1}{(a+z)} + f(x,\theta)$$

It follows that

$$f(x,\theta) = \frac{1}{a}\left(\bar{v} + \frac{\partial \bar{w}}{\partial \theta}\right)$$

Thus

$$v = \bar{v}\left(1 + \frac{z}{a}\right) - \left(\frac{z}{a}\right)\left(\frac{\partial \bar{w}}{\partial \theta}\right) \tag{2.7b}$$

Similarly requiring the shearing strain ϵ_{zx} to vanish yields

$$u = \bar{u} - z\frac{\partial \bar{w}}{\partial x} \tag{2.7c}$$

The strain components are now expressed in terms of midsurface quantities by substituting (2.7) into (2.1), (2.2), and (2.4). Further, $(a+z)^{-1}$ and $(a+z)^{-2}$ are replaced by expansions of z up to and including second-order terms. The resulting expressions are

$$\epsilon_x = \bar{\epsilon}_x + z\kappa_x \tag{2.8a}$$

$$\epsilon_\theta = \bar{\epsilon}_\theta + z\kappa_\theta + z^2\mu_\theta \tag{2.8b}$$

$$\epsilon_{x\theta} = \bar{\epsilon}_{x\theta} + z\kappa_{x\theta} + z^2\mu_{x\theta} \tag{2.8c}$$

where

$$\bar{\epsilon}_x = \frac{\partial \bar{u}}{\partial x} + \frac{1}{2}\left(\frac{\partial \bar{w}}{\partial x}\right)^2 \tag{2.9a}$$

$$\kappa_x = -\frac{\partial^2 \bar{w}}{\partial x^2} \tag{2.9b}$$

$$\bar{\epsilon}_\theta = \frac{1}{a}\left[\bar{w} + \frac{\partial \bar{v}}{\partial \theta} + \frac{1}{2a}\left(\frac{\partial \bar{w}}{\partial \theta}\right)^2\right] \tag{2.9c}$$

$$\kappa_\theta = -\frac{1}{a^2}\left[\bar{w} + \frac{\partial^2 \bar{w}}{\partial \theta^2} + \frac{1}{a}\left(\frac{\partial \bar{w}}{\partial \theta}\right)^2\right] \tag{2.9d}$$

$$\mu_\theta = \frac{1}{a^3}\left[\bar{w} + \frac{\partial^2 \bar{w}}{\partial\theta^2} + \frac{3}{2a}\left(\frac{\partial \bar{w}}{\partial\theta}\right)^2\right] \tag{2.9e}$$

$$\bar{\epsilon}_{x\theta} = \left[\frac{\partial \bar{v}}{\partial x} + \frac{1}{a}\frac{\partial \bar{u}}{\partial\theta} + \frac{1}{a}\frac{\partial \bar{w}}{\partial x}\frac{\partial \bar{w}}{\partial\theta}\right] \tag{2.9f}$$

$$\kappa_{x\theta} = \frac{1}{a}\left[\frac{\partial \bar{v}}{\partial x} - 2\frac{\partial^2 \bar{w}}{\partial x\partial\theta} - \frac{1}{a}\frac{\partial \bar{u}}{\partial\theta} - \frac{1}{a}\frac{\partial \bar{w}}{\partial x}\frac{\partial \bar{w}}{\partial\theta}\right] \tag{2.9g}$$

$$\mu_{x\theta} = \frac{1}{a^2}\left[\frac{1}{a}\frac{\partial \bar{u}}{\partial\theta} + \frac{\partial^2 \bar{w}}{\partial x\partial\theta} + \frac{1}{a}\frac{\partial \bar{w}}{\partial x}\frac{\partial \bar{w}}{\partial\theta}\right] \tag{2.9h}$$

B. ENERGY OF THE SYSTEM

Since the material is assumed to be isotropic and linearly elastic with modulus of elasticity E and Poisson's ratio ν, the strain energy has the form

$$U = \frac{E}{(1-\nu^2)}\int_0^{2\pi}\int_0^{\ell}\int_{-h/2}^{h/2}\left[\epsilon_x^2 + \epsilon_\theta^2 + 2\nu\epsilon_x\epsilon_\theta + \frac{(1-\nu)}{2}\epsilon_{x\theta}^2\right](a+z)\,dz\,dx\,d\theta \tag{2.10}$$

The integration over the thickness can be carried out after substituting from Eqs. (2.8). Consistent with the retention of second-order thickness terms in (2.8), fifth-order terms are discarded here. Then

$$\begin{aligned} U = \frac{E}{2(1-\nu^2)}\int_0^{2\pi}\int_0^{\ell}\Bigg\langle & a\Bigg\{h\left[\bar{\epsilon}^2 + \bar{\epsilon}^2 + 2\nu\bar{\epsilon}\,\bar{\epsilon} + \frac{(1-\nu)}{2}\bar{\epsilon}_{x\theta}^2\right] \\ & + \frac{h^3}{12}\left[\kappa_x^2 + \kappa_\theta^2 + 2\mu_\theta\bar{\epsilon}_\theta + 2\nu\bar{\epsilon}_x\mu_\theta + 2\nu\kappa_x\kappa_\theta\right. \\ & \left. + \frac{(1-\nu)}{2}\left(\kappa_{x\theta}^2 + 2\bar{\epsilon}_{x\theta}\mu_{x\theta}\right)\right]\Bigg\} \\ & + \frac{h^2}{12}\left[2\bar{\epsilon}_x\kappa_x + 2\bar{\epsilon}_\theta\kappa_\theta + 2\nu\bar{\epsilon}_x\kappa_\theta + 2\nu\bar{\epsilon}_\theta\kappa_x\right. \\ & \left. + (1-\nu)\bar{\epsilon}_{x\theta}\kappa_{x\theta}\right]\Bigg\rangle\,dx\,d\theta \end{aligned} \tag{2.11}$$

Equation (2.11) may be rewritten in terms of midsurface displacements using Eqs. (2.9). The result is simplified slightly by neglecting the square of the thickness-to-radius ratio compared to unity. With this, the strain energy can be separated into its membrane and bending components. Thus

$$U = U_m + U_b$$

where

$$U_m = \frac{K}{2}\int_0^{2\pi}\int_0^{\ell}\left[\left(a\bar{u}_x^2 + \frac{\bar{v}_\theta^2}{a} + \frac{\bar{w}^2}{a} + 2\frac{\bar{w}\bar{v}_\theta}{a} + a\bar{u}_x\bar{w}_x^2 + \frac{\bar{v}_\theta\bar{w}_\theta^2}{a} + \frac{\bar{w}\bar{w}_\theta^2}{a}\right)\right.$$
$$+ \nu\left(2\bar{u}_x\bar{v}_\theta + 2\bar{u}_x\bar{w} + \frac{\bar{u}_x\bar{w}_\theta^2}{a} + \bar{v}_\theta\bar{w}_x^2 + \bar{w}\bar{w}_x^2\right)$$
$$\left.+ (1-\nu)\left(\frac{\bar{u}_\theta^2}{2a} + \frac{a\bar{v}_x^2}{2} + \bar{u}_\theta\bar{v}_x + \frac{\bar{u}_\theta\bar{w}_x\bar{w}_\theta}{a} + \bar{v}_x\bar{w}_x\bar{w}_\theta\right)\right] dx d\theta \qquad (2.12a)$$

$$U_b = \frac{D}{2}\int_0^{2\pi}\int_0^{\ell}\left[\left(-2\bar{u}_x\bar{w}_{xx} + a\bar{w}_{xx}^2 + \frac{\bar{w}_{\theta\theta}^2}{a^3} + 2\frac{\bar{w}\bar{w}_{\theta\theta}}{a^3} + 2\frac{\bar{w}_{\theta\theta}\bar{w}_\theta^2}{a^4}\right.\right.$$
$$\left.- \bar{w}_{xx}\bar{w}_x^2\right) + \nu\left(2\frac{\bar{w}_{xx}\bar{w}_{\theta\theta}}{a} - 2\frac{\bar{v}_\theta\bar{w}_{xx}}{a} + \frac{\bar{w}_{xx}\bar{w}_\theta}{a^2}\right)$$
$$\left.+ (1-\nu)\left(\frac{\bar{u}_\theta\bar{w}_{x\theta}}{a^2} - 3\frac{\bar{v}_x\bar{w}_{x\theta}}{a} + 2\frac{\bar{w}_{x\theta}^2}{a} + \frac{\bar{w}_{x\theta}\bar{w}_x\bar{w}_\theta}{a^2}\right)\right] dx d\theta \qquad (2.12b)$$

$$K = Eh/(1-\nu^2) \qquad (2.13a)$$

$$D = Eh^3/12(1-\nu^2) \qquad (2.13b)$$

In (2.12) a subscript denotes partial differentiation with respect to the coordinate.

The kinetic energy is

$$T = \frac{1}{2}\rho \int_0^{2\pi}\int_0^{\ell}\int_{-h/2}^{h/2} \left[\left(\frac{\partial u}{\partial t}\right)^2 + \left(\frac{\partial v}{\partial t}\right)^2 + \left(\frac{\partial w}{\partial t}\right)^2\right](a+z)\,dz\,dx\,d\theta \qquad (2.14a)$$

where ρ and t denote the material density and time, respectively. Introducing the midsurface expressions, performing the integration through the thickness, and neglecting terms that involve the thickness-to-radius ratio gives

$$T = \rho \frac{h}{2} \int_0^{2\pi}\int_0^{\ell} \left[\left(\frac{\partial \bar{u}}{\partial t}\right)^2 + \left(\frac{\partial \bar{v}}{\partial t}\right)^2 + \left(\frac{\partial \bar{w}}{\partial t}\right)^2\right] dx\, d\theta \qquad (2.14b)$$

C. EQUATIONS OF MOTION

The three displacement components are expressed as double Fourier series having time-dependent coefficients. Their expansions are

$$\bar{u} = \sum_{m=1}^{\infty} U_{mo}(t) \sin\frac{m\pi x}{\ell} + \sum_{m=1}^{\infty}\sum_{n=1}^{\infty} U_{mn}(t) \sin\frac{m\pi x}{\ell} \cos n\theta \qquad (2.15a)$$

$$\bar{v} = \sum_{n=1}^{\infty} V_{on}(t) \sin n\theta + \sum_{m=1}^{\infty}\sum_{n=1}^{\infty} V_{mn}(t)\cos\frac{m\pi x}{\ell} \sin n\theta \qquad (2.15b)$$

$$\bar{w} = W_{oo}(t) + \sum_{m=1}^{\infty} W_{mo}(t) \cos\frac{m\pi x}{\ell} + \sum_{n=1}^{\infty} W_{on}(t)\cos n\theta + \sum_{m=1}^{\infty}\sum_{n=1}^{\infty} W_{mn}(t) \cos\frac{m\pi x}{\ell} \cos n\theta \qquad (2.15c)$$

At each boundary of the shell, the slope $\partial\bar{w}/\partial x$ and the axial displacement vanish while the radial and circumferential displacements do not. The effective radial and circumferential shear per unit length are zero at the boundaries. Although these boundary conditions appear arcane, in the present problem they give rise to energy expressions which are more tractable than

those following from more common geometric constraints. Thus they permit the analysis of finite length shells without undue complication.

The energy is expressed in terms of the Fourier coefficients by substituting Eqs. (2.15) into (2.12) and (2.14b) and integrating over the mid-surface. Treating the coefficients as generalized coordinates, the associated Lagrange equations are three systems of second order, ordinary, nonlinear differential equations for the U, V, and W terms. Each equation is coupled internally to members of its system and externally to members of the other two systems. Reasonable approximations must be made before useful solutions can be obtained. For this reason an analysis of the linear problem is undertaken in the following chapter.

CHAPTER III

ANALYSIS OF THE LINEAR PROBLEM

A. SOLUTION FOR THE DISPLACEMENTS

The analysis of the nonlinear problem is facilitated by the use of uncoupling conditions for the differential equations. Such conditions can be obtained by introducing approximate relations between the tangential and radial Fourier coefficients. To determine the validity of these relations, the response of the shell governed by linear equations of motion is considered here. Approximate solutions obtained by introducing two different uncoupling relations are compared to the exact solution. In both cases excellent agreement is found for purely radial loading.

As discussed in Chapter II, Lagrange equations can be written for the Fourier coefficients U_{mn}, V_{mn}, and W_{mn}. Neglecting quadratic terms in the coefficients, these equations are

$$\ddot{U}_{mn} + \left[\pi^2 m^2 \left(\frac{a}{\ell}\right)^2 + \frac{(1-\nu)}{2} n^2\right] U_{mn} + \frac{\pi(1+\nu)mn}{2}\left(\frac{a}{\ell}\right) V_{mn} + \left[\pi\nu m\left(\frac{a}{\ell}\right) + \frac{\pi^2 m^3}{12}\left(\frac{h}{a}\right)^2\left(\frac{a}{\ell}\right)^3 - \frac{\pi(1-\nu)mn^2}{24}\left(\frac{h}{a}\right)^2\left(\frac{a}{\ell}\right)\right] W_{mn} = 0 \tag{3.1a}$$

$$\ddot{V}_{mn} + \left[n^2 + \frac{\pi^2(1-\nu)m^2}{2}\left(\frac{a}{\ell}\right)^2\right] V_{mn} + \frac{\pi(1+\nu)mn}{2}\left(\frac{a}{\ell}\right) U_{mn} + \left[n + \frac{\pi^2(3-\nu)m^2 n}{24}\left(\frac{h}{a}\right)^2\left(\frac{a}{\ell}\right)^2\right] W_{mn} = 0 \tag{3.1b}$$

$$\ddot{W}_{mn} + \left[\pi\nu m\left(\frac{a}{\ell}\right) + \frac{\pi^3 m^3}{12}\left(\frac{h}{a}\right)^2\left(\frac{a}{\ell}\right)^3 - \frac{\pi(1-\nu)mn^2}{24}\left(\frac{h}{a}\right)^2\left(\frac{a}{\ell}\right)\right] U_{mn} + \left[n + \frac{\pi^2(3-\nu)m^2 n}{24}\right.$$

$$\left.(x)\ \left(\frac{h}{a}\right)^2\left(\frac{a}{\ell}\right)^2\right] V_{mn} + \left[1 + \frac{\pi^4 m^4}{12}\left(\frac{h}{a}\right)^2\left(\frac{a}{\ell}\right)^4 + \frac{n^2(n^2-2)}{12}\left(\frac{h}{a}\right)^2 + \frac{\pi^2 m^2 n}{6}\right.$$

$$\left.(x)\ \left(\frac{h}{a}\right)^2\left(\frac{a}{\ell}\right)^2\right] W_{mn} = 0 \qquad (3.1c)$$

where

$$(\dot{}) = d(\ )/d\tau$$

$$\tau = ct/a$$

$$c = [E/\rho(1-\nu^2)]^{1/2}$$

Equations (3.1) will be rewritten as

$$\ddot{U}_{mn} + C_1 U_{mn} + C_2 V_{mn} + C_3 W_{mn} = 0 \qquad (3.2a)$$

$$\ddot{V}_{mn} + C_4 V_{mn} + C_2 U_{mn} + C_5 W_{mn} = 0 \qquad (3.2b)$$

$$\ddot{W}_{mn} + C_6 W_{mn} + C_3 U_{mn} + C_5 V_{mn} = 0 \qquad (3.2c)$$

where

$$C_1 = \frac{n^2}{3} + \pi^2 m^2\left(\frac{a}{\ell}\right)^2 \qquad (3.3a)$$

$$C_2 = \frac{2\pi mn}{3}\left(\frac{a}{\ell}\right) \qquad (3.3b)$$

$$C_3 = \frac{\pi m}{3}\left(\frac{a}{\ell}\right) + \frac{\pi^3 m^3}{3}\left(\frac{h}{a}\right)^2\left(\frac{a}{\ell}\right)^3 - \frac{\pi mn^2}{36}\left(\frac{h}{a}\right)^2\left(\frac{a}{\ell}\right) \qquad (3.3c)$$

$$C_4 = n^2 + \frac{\pi^2 m^2}{3}\left(\frac{a}{\ell}\right)^2 \qquad (3.3d)$$

$$C_5 = n + \frac{\pi^2 m^2 n}{9}\left(\frac{h}{a}\right)^2\left(\frac{a}{\ell}\right)^2 \qquad (3.3e)$$

$$C_6 = 1 + \frac{\pi^4 m^4}{12}\left(\frac{h}{a}\right)^2\left(\frac{a}{\ell}\right)^4 + \frac{n^4}{12}\left(\frac{h}{a}\right)^2 - \frac{n^2}{6}\left(\frac{h}{a}\right)^2 + \frac{\pi^2 m^2 n^2}{6}\left(\frac{h}{a}\right)^2\left(\frac{a}{\ell}\right)^2 \qquad (3.3f)$$

in which Poisson's ratio has been taken as 1/3.

The solutions are simple harmonic functions of time. Introducing this form into the differential equations leads to the frequency equation

$$F^6 - (C_1+C_4+C_6)F^4 + (C_1C_4+C_1C_6+C_4C_6-C_2^2-C_3^2-C_5^2)F^2 + (-C_1C_4C_6+C_1C_5^2+C_6C_2^2-2C_2C_3C_5+C_4C_3^2) = 0 \qquad (3.4)$$

In increasing magnitude, F_1, F_2, and F_3 will denote the three distinct frequencies for each m and n. Generally the frequencies F_2 and F_3 are of comparable magnitude, being both much larger than F_1 and insensitive to changes in the shell thickness. The lowest frequency depends upon the radius-to-thickness ratio. In Fig. 2 the three frequencies are displayed on a logarithmic scale as functions of a/h for a number of modes.

If the shell is subjected to a radial impulse, the three displacement components and the tangential velocities are initially zero. This requires

$$U_{mn}(o) = V_{mn}(o) = W_{mn}(o) = \dot{U}_{mn}(o) = \dot{V}_{mn}(o) = 0 \qquad (3.5a)$$

The value of $\dot{W}_{mn}(o)$ can be obtained from the initial radial velocity

$$\dot{w}(x,\theta,o) = \sum_{m=0}^{\infty}\sum_{n=0}^{\infty} \dot{W}_{mn}(o)\cos\frac{m\pi x}{\ell}\cos n\theta = f(x,\theta) \qquad (3.5b)$$

In general $f(x,\theta)$ would be derived from the initial impulse. In the work that

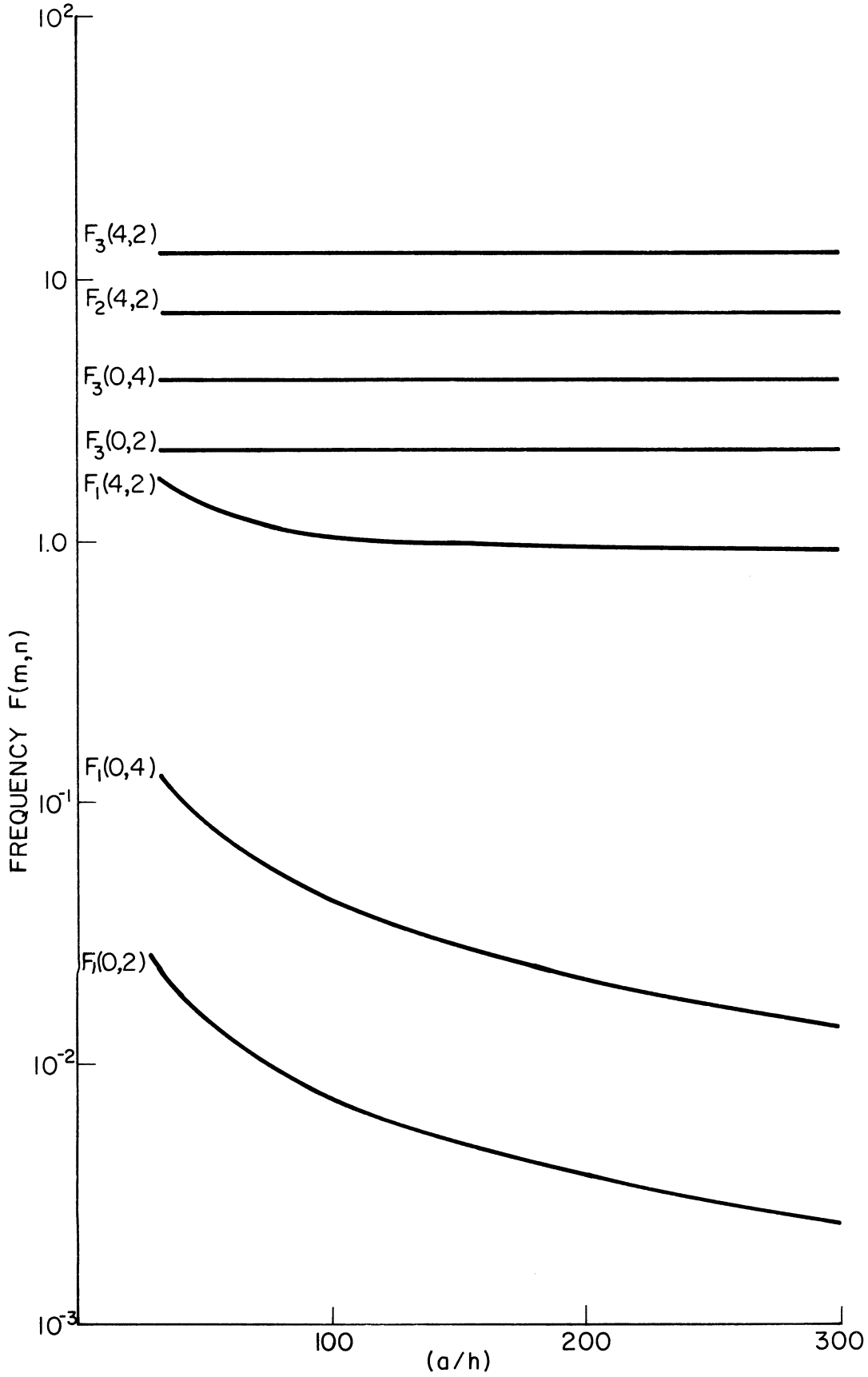

Fig. 2. Three frequencies of the linear problem vs. radius-to-thickness ratio.

follows it will be treated as a given initial velocity.

Under these conditions, the solution to Eqs. (3.2) is

$$U_{mn} = A_1 \sin F_1\tau + A_4 \sin F_2\tau + A_7 \sin F_3\tau \tag{3.6a}$$

$$V_{mn} = A_2 \sin F_1\tau + A_5 \sin F_2\tau + A_8 \sin F_3\tau \tag{3.6b}$$

$$W_{mn} = A_3 \sin F_1\tau + A_6 \sin F_2\tau + A_9 \sin F_3\tau \tag{3.6c}$$

where

$$A_1 = \dot{W}_{mn}(o)F_2F_3C_9(C_{10}-C_8)/C_7 \tag{3.6d}$$

$$A_2 = \dot{W}_{mn}(o)F_2F_3(C_{10}-C_8)/C_7 \tag{3.6e}$$

$$A_3 = \dot{W}_{mn}(o)F_2F_3C_{12}(C_8-C_9)/C_7 \tag{3.6f}$$

$$A_4 = \dot{W}_{mn}(o)F_1F_3C_{10}(C_8-C_9)/C_7 \tag{3.6g}$$

$$A_5 = \dot{W}_{mn}(o)F_1F_3(C_8-C_9)/C_7 \tag{3.6h}$$

$$A_6 = \dot{W}_{mn}(o)F_1F_3C_{13}(C_9-C_8)/C_7 \tag{3.6i}$$

$$A_7 = \dot{W}_{mn}(o)F_1F_2C_8(C_9-C_{10})/C_7 \tag{3.6j}$$

$$A_8 = \dot{W}_{mn}(o)F_1F_2(C_9-C_{10})/C_7 \tag{3.6k}$$

$$A_9 = \dot{W}_{mn}(o)F_1F_2C_{11}(C_{10}-C_9)/C_7 \tag{3.6\ell}$$

$$C_7 = F_1F_2F_3[C_{11}(C_{10}-C_9) + C_{12}(C_8-C_{10}) + C_{13}(C_9-C_8)] \tag{3.6m}$$

$$C_8 = [(C_1-F_3^2)C_5-C_2C_3]/[(C_4-F_3^2)C_3-C_2C_5] \tag{3.6n}$$

$$C_9 = [C_2C_3-(C_1-F_1^2)C_5]/[C_2C_5-(C_4-F_1^2)C_3] \tag{3.6o}$$

$$C_{10} = [C_2C_3-(C_1-F_2^2)C_5]/[C_2C_5-(C_4-F_2^2)C_3] \tag{3.6p}$$

$$C_{11} = (C_2C_8+C_1-F_3^2)/C_3 \tag{3.6q}$$

$$C_{12} = (C_2C_9+C_1-F_1^2)/C_3 \tag{3.6r}$$

$$C_{13} = (C_2C_{10}+C_1-F_2^2)/C_3 \tag{3.6s}$$

In general the amplitude of a low frequency component such as A_3, is much larger than the amplitudes of the companion high frequency components such as A_6 and A_9. This is shown in Fig. 3. As previously mentioned, the amplitudes A_3, A_6, and A_9 of the radial coefficient W_{mn} are greater than the corresponding amplitudes of the tangential coefficients U_{mn} and V_{mn}. A comparison of the largest amplitudes A_1, A_2, and A_3 is made in Fig. 4 for a number of modes. Similar observations have been made by Arnold and Warburton.[4]

B. APPROXIMATE SOLUTION NEGLECTING HIGH FREQUENCY TERMS

The differential equations of the nonlinear problem may be uncoupled by defining a dependence of U_{mn} and V_{mn} upon W_{mn}. The high frequency terms make a negligible contribution to the total displacement of the shell and can be discarded. Thus the first approximation considered is to assume that the Fourier coefficients are related in the same manner as the amplitudes of their largest components A_1, A_2, and A_3. The exact linear solution requires that

$$A_1 = -A_3/C_{12} \tag{3.7a}$$

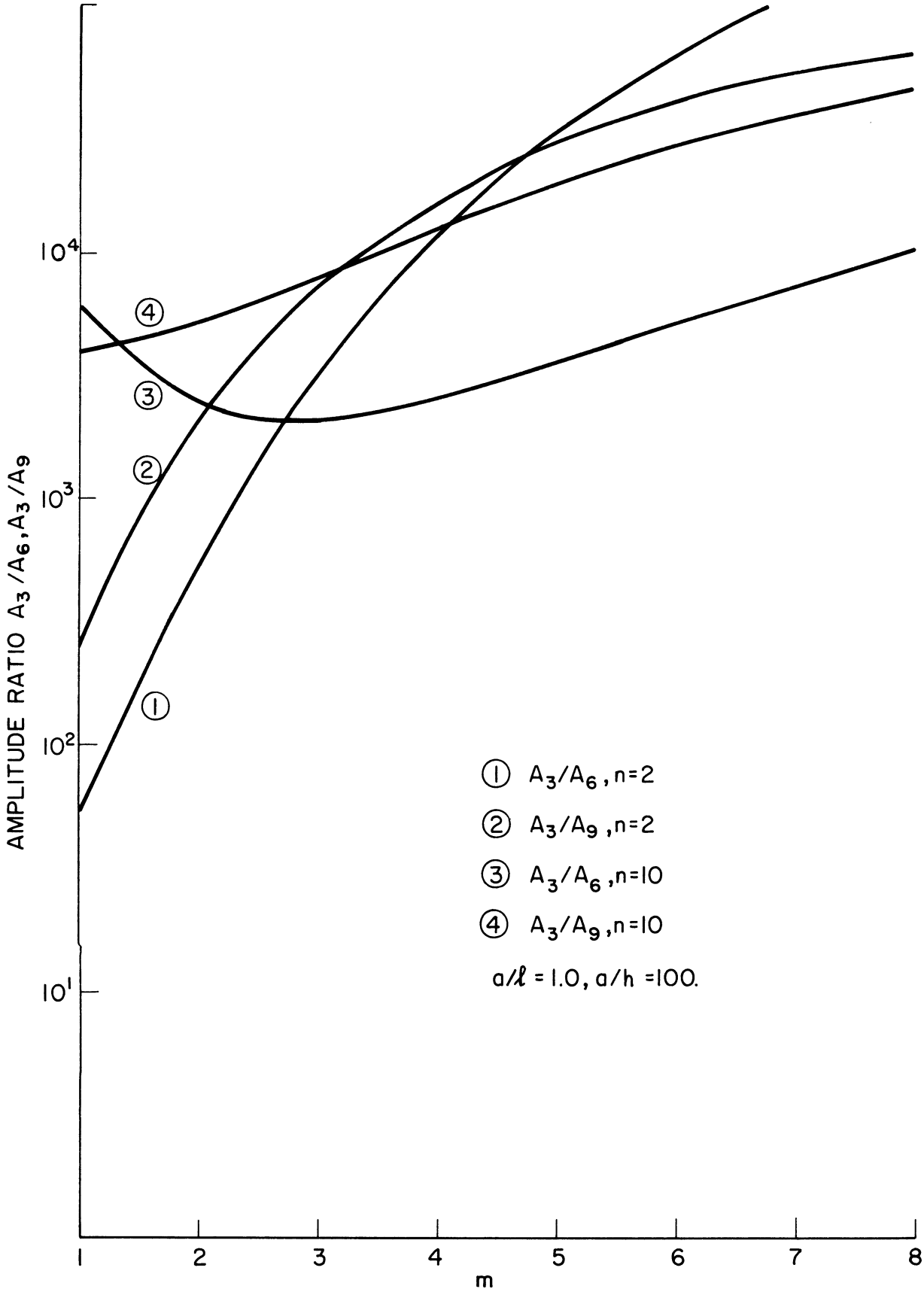

Fig. 3. Ratios of the amplitudes of the high frequency to low frequency components of W_{mn} vs. longitudinal wave number.

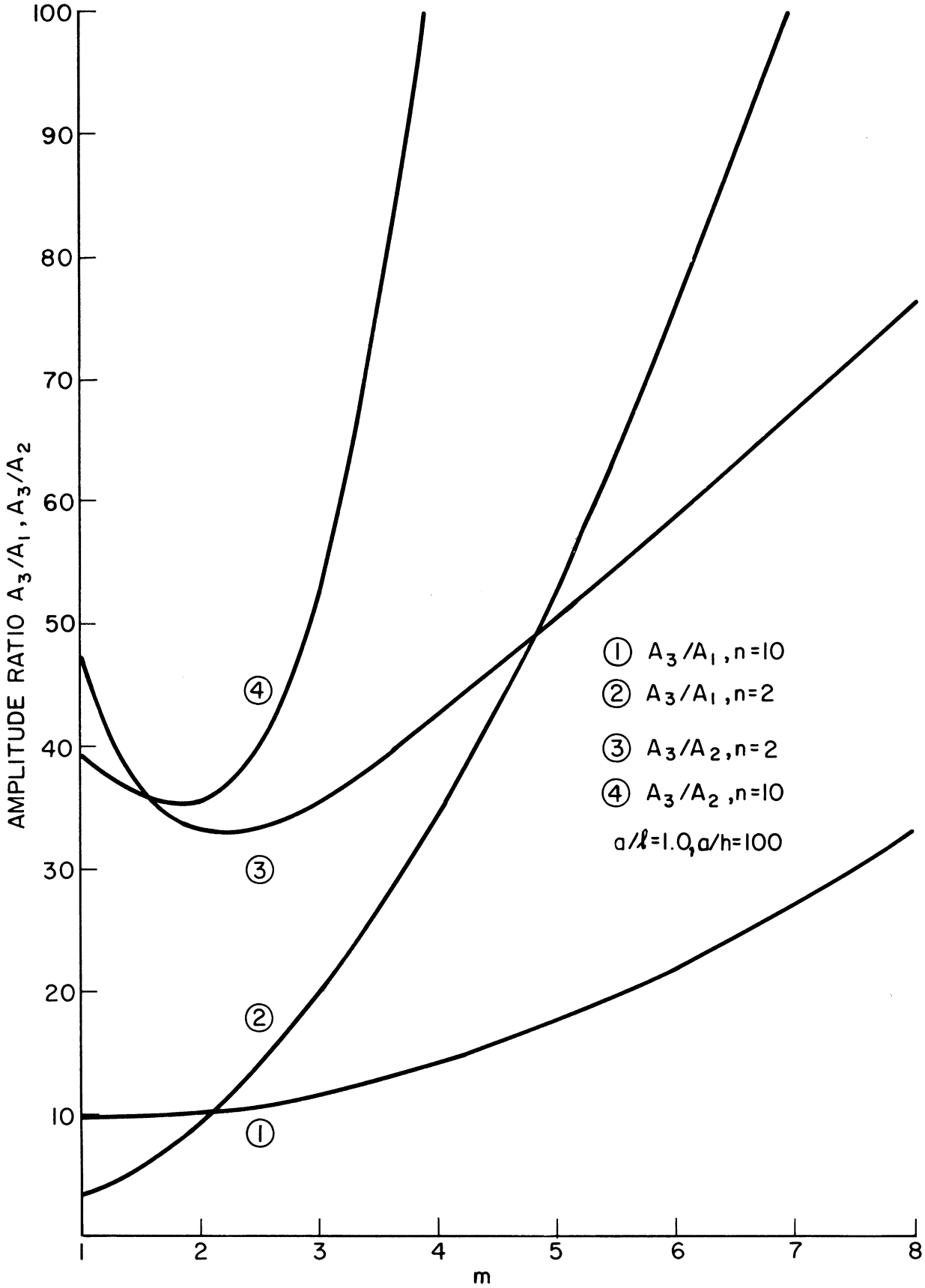

Fig. 4. Ratios of the largest amplitude of U_{mn} and V_{mn} that of W_{mn} vs. longitudinal wave number.

$$A_2 = -A_3C_9/C_{12} \tag{3.7b}$$

where C_9 and C_{12} are defined in (3.6).

The approximation is

$$U_{mn}/W_{mn} = A_1/A_3 = -1/C_{12} \tag{3.8a}$$

$$V_{mn}/W_{mn} = A_2/A_3 = -C_9/C_{12} \tag{3.8b}$$

The relationships (3.8) can be substituted into the differential equation for W_{mn} to obtain

$$\ddot{W}_{mn} + (C_6-C_3/C_{12}-C_5C_9/C_{12})W_{mn} = 0 \tag{3.9a}$$

The initial radial displacement is zero, requiring $W_{mn}(o)$ to vanish. The value of $\dot{W}_{mn}(o)$ can be obtained from the initial radial velocity (3.5b). With these conditions, the solution to (3.9a) is

$$W_{mn} = \frac{\dot{W}_{mn}(o)}{\tilde{F}} \sin \tilde{F}\tau \tag{3.9b}$$

where

$$\tilde{F} = (C_6-C_3/C_{12}-C_5C_9/C_{12})^{1/2} \tag{3.9c}$$

From (3.8), the longitudinal and circumferential coefficients are

$$U_{mn} = -\frac{\dot{W}_{mn}(o)}{\tilde{F}C_{12}} \sin \tilde{F}\tau \tag{3.9d}$$

$$V_{mn} = -\frac{\dot{W}_{mn}(o)}{\tilde{F}C_{12}} C_9 \sin \tilde{F}\tau \tag{3.9e}$$

The amplitudes and frequency of (3.9) are compared to the three largest amplitudes and lowest frequency of the exact linear solution in Figs. 5 and 6, respectively. The modes chosen span a range that will be of interest in the work that follows.

C. APPROXIMATE SOLUTION NEGLECTING IN-PLANE INERTIA

A second approximation can be used for uncoupling the differential equations. For the geometry and loading considered, the response is characterized by a strong radial motion; this suggests neglecting tangential inertia terms in the equations of motion. This approximation was introduced by Reissner.[5] With this simplification, the linear differential equations (3.2) become

$$C_1 U_{mn} + C_2 V_{mn} + C_3 W_{mn} = 0 \tag{3.10a}$$

$$C_4 V_{mn} + C_2 U_{mn} + C_5 W_{mn} = 0 \tag{3.10b}$$

$$\ddot{W}_{mn} + C_6 W_{mn} + C_3 U_{mn} + C_5 V_{mn} = 0 \tag{3.10c}$$

These can be rewritten as

$$U_{mn} = W_{mn}(C_2C_5 - C_3C_4)/(C_1C_4 - C_2^2) \tag{3.10d}$$

$$V_{mn} = W_{mn}(C_2C_3 - C_1C_5)/(C_1C_4 - C_2^2) \tag{3.10e}$$

$$\ddot{W}_{mn} + \tilde{\tilde{F}}^2 W_{mn} = 0 \tag{3.10f}$$

where

$$\tilde{\tilde{F}} = [C_6 - C_3^2/C_1 + (C_2C_3 - C_1C_5)^2/C_1(C_2^2 - C_1C_4)]^{1/2} \tag{3.10g}$$

The initial conditions are the same as in the approximation of the preceding article, that is, a zero value for $W_{mn}(o)$ and a definite value for $\dot{W}_{mn}(o)$. The solution to (3.10) is

$$W_{mn} = \frac{\dot{W}_{mn}(o)}{\tilde{\tilde{F}}} \sin \tilde{\tilde{F}}\tau \tag{3.11a}$$

$$U_{mn} = \frac{(C_2C_5-C_3C_4)\dot{W}_{mn}(o)}{(C_1C_4-C_2^2)\tilde{\tilde{F}}} \sin \tilde{\tilde{F}}\tau \tag{3.11b}$$

$$V_{mn} = \frac{(C_2C_3-C_1C_5)\dot{W}_{mn}(o)}{(C_1C_4-C_2^2)\tilde{\tilde{F}}} \sin \tilde{\tilde{F}}\tau \tag{3.11c}$$

The radial Fourier coefficients and frequencies obtained from this approximation and that of the preceding article are compared to the exact results in Figs. 5 and 6. The two approximations give very comparable results for the frequencies. Both approximations give very good results for the amplitudes with the second approximation uniformly producing one half of the error of the first approximation. Thus for the analysis of the nonlinear problem tangential inertia is neglected.

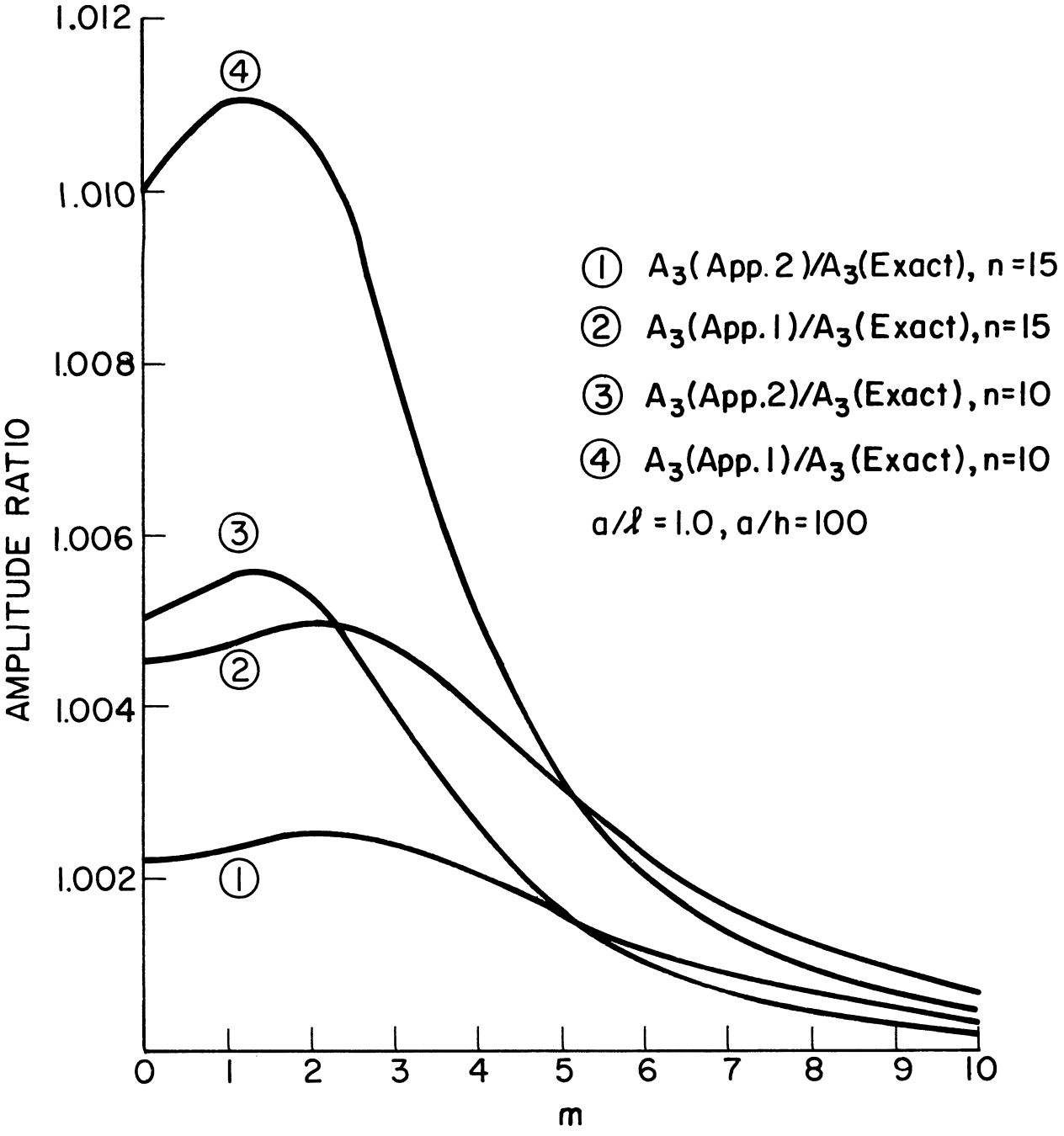

Fig. 5. Ratios of approximate amplitudes to exact amplitudes vs. the longitudinal wave number.

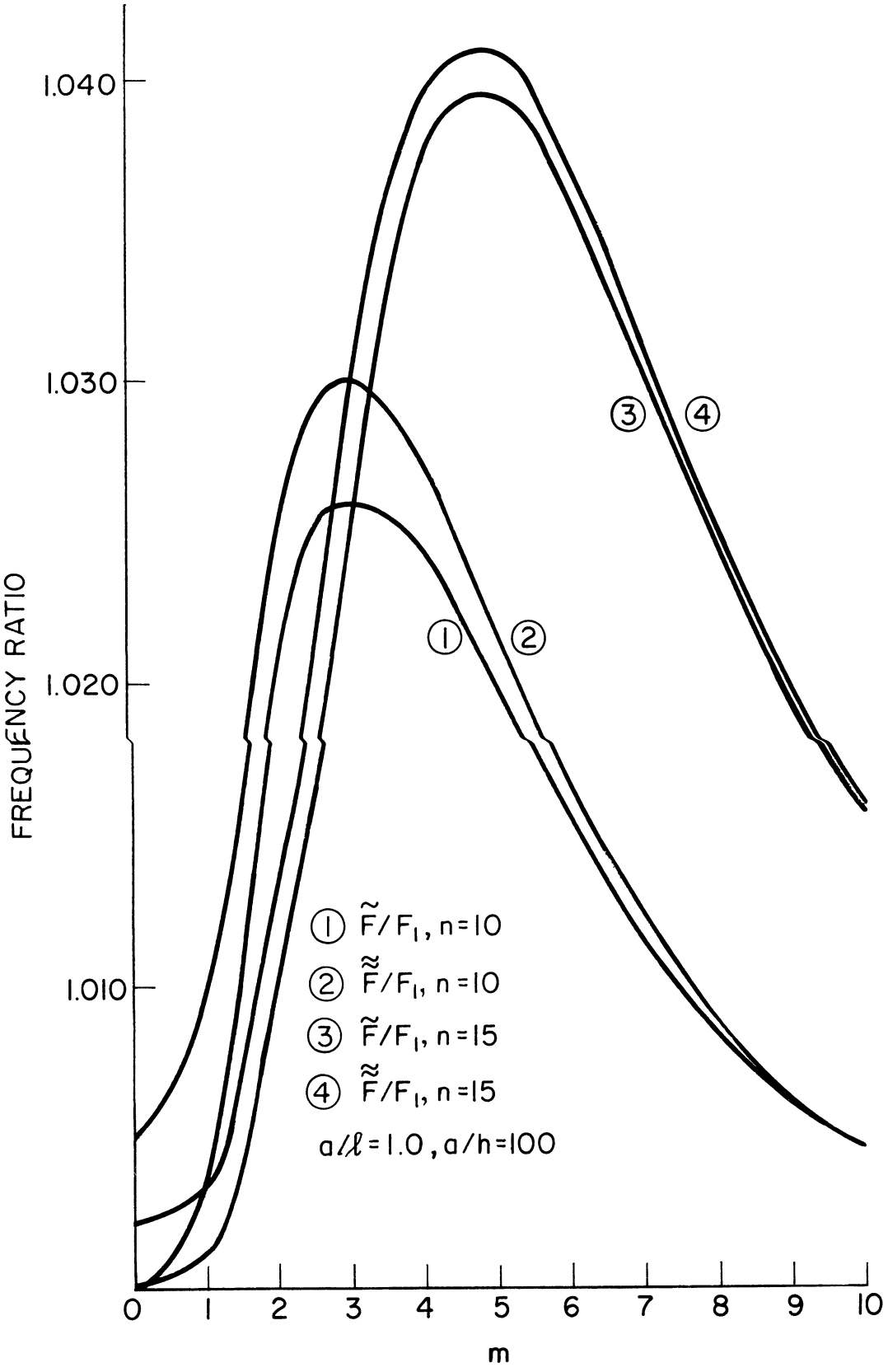

Fig. 6. Ratios of approximate frequencies to exact frequencies vs. the longitudinal wave number.

CHAPTER IV

SOLUTION OF THE NONLINEAR PROBLEM

In this chapter both the stability of the response to a uniform impulsive pressure and the long term motion of the shell are considered. If the initial, nearly uniform, radial impulse is of a sufficiently short duration, it can be considered equivalent to an initial, nearly uniform, radial velocity, i.e., a uniform velocity with a superimposed spatial perturbation. For small values of time the growth characteristics of the displacements are examined. The basic response is considered stable if the motion associated with the perturbation remains of perturbational magnitude. The fundamental motion is unstable if a growth in one or more of the perturbed modes is predicted. For the long term study it is assumed that the modes exhibiting growth characterize the response of the shell. If a mode remains of perturbational size in the initial analysis, it will be neglected in the long term study.

A. SHORT TERM ANALYSIS

The nonzero initial conditions can be expressed as

$$\frac{\dot{W}_{oo}(o)}{a} = \frac{v_o}{c}, \quad \frac{\dot{W}_{mn}(o)}{a} = \frac{v_o}{c}\epsilon_{mn} \tag{4.1}$$

where $v_o \ll c$ and $\epsilon_{mn} \ll 1$ for all pairs of m and n except (o,o); v_o is the initial uniform radial velocity imparted to the shell.

The differential equation for the basic response as affected by the perturbation is

$$\frac{\ddot{W}_{oo}}{a} + \frac{W_{oo}}{a} + \frac{1}{4}\left[\sum_{j=1}^{\infty} j^2\left(\frac{W_{oj}}{a}\right)^2 + \frac{\pi^2}{3}\left(\frac{a}{\ell}\right)^2 \sum_{i=1}^{\infty} i^2\left(\frac{W_{io}}{a}\right)^2\right.$$

$$\left.\frac{1}{2}\sum_{i=1}^{\infty}\sum_{j=1}^{\infty} j^2\left(\frac{W_{ij}}{a}\right)^2 + \frac{\pi^2}{6}\left(\frac{a}{\ell}\right)^2 \sum_{i=1}^{\infty}\sum_{j=1}^{\infty} i^2\left(\frac{W_{ij}}{a}\right)^2\right] = 0 \qquad (4.2)$$

For small values of time, the summations appearing in (4.2) involve products of coefficients of perturbational magnitude and may be neglected. With initial conditions (4.1), the solution is the basic response

$$W_{oo}(\tau) = \frac{v_o a}{c}\sin\tau \qquad (4.3)$$

Using the energy expressions of Chapter II, the Lagrange equation for W_{mn} is

$$\frac{\ddot{W}_{mn}}{a} + \frac{W_{mn}}{a}\left[1 + \frac{\pi^4 m^4}{12}\left(\frac{h}{a}\right)^2\left(\frac{a}{\ell}\right)^4 + \frac{n^4}{12}\left(\frac{h}{a}\right)^2 - \frac{n^2}{6}\left(\frac{h}{a}\right)^2 + \frac{\pi^2 m^2 n^2}{6}\left(\frac{h}{a}\right)\left(\frac{a}{\ell}\right)^2\right]$$

$$+ U_{mn}\left[\frac{\pi m}{3}\left(\frac{a}{\ell}\right) + \frac{\pi^3 m^3}{12}\left(\frac{h}{a}\right)^2\left(\frac{a}{\ell}\right)^3 - \frac{\pi m n^2}{36}\left(\frac{h}{a}\right)^2\left(\frac{a}{\ell}\right)\right]$$

$$+ \frac{V_{mn}}{a}\left[n + \frac{\pi^2 m^2 n}{9}\left(\frac{h}{a}\right)^2\left(\frac{a}{\ell}\right)^2\right] + \left(\frac{W_{on}W_{mo}}{a^2} + \frac{W_{oo}W_{mn}}{a^2}\right)\left(n^2 + m^2\frac{\pi^2 a^2}{3\ell^2}\right)$$

$$+ \frac{1}{2}\left[\sum_{i=1}^{\infty}\frac{W_{io}W_{m+i,n}}{a^2}\left(n^2 + \frac{\pi^2 m^2 a^2}{3\ell^2} + \frac{\pi^2 i m a^2}{3\ell^2} + \frac{\pi^2 i^2 a^2}{3\ell^2}\right)\right.$$

$$+ \sum_{i=1}^{m-1}\frac{W_{io}W_{m-i,n}}{a^2}\left(n^2 + \frac{\pi^2 m^2 a^2}{3\ell^2} - \frac{\pi^2 i m a^2}{3\ell^2} + \frac{\pi^2 i^2 a^2}{3\ell^2}\right)$$

$$\left. + \sum_{i=1}^{\infty}\frac{W_{in}W_{i+m,o}}{a^2}\left(n^2 + \frac{\pi^2 m^2 a^2}{3\ell^2} + \frac{\pi^2 i m a^2}{3\ell^2} + \frac{\pi^2 i^2 a^2}{3\ell^2}\right)\right]$$

$$+ \frac{1}{4}\left\{\sum_{i=1}^{\infty}\sum_{j=1}^{\infty}\frac{W_{ij}W_{i+m,j+n}}{a^2}\left[j^2 + jn + n^2 + \frac{\pi^2 a^2}{3\ell^2}(im + i^2 + m^2)\right]\right.$$

$$\left. + \sum_{i=1}^{\infty}\sum_{j=n+1}^{\infty}\frac{W_{ij}W_{i+m,j-n}}{a^2}\left[j^2 - jn + n^2 + \frac{\pi^2 a^2}{3\ell^2}(im + i^2 + m^2)\right]\right.$$

$$+ \sum_{i=1}^{\infty} \sum_{j=1}^{n-1} \frac{W_{ij}W_{i+m,n-j}}{a^2} \left[j^2 - jn + n^2 + \frac{\pi^2 a^2}{3\ell^2} (im+i^2+m^2) \right]$$

$$+ \sum_{i=1}^{m-1} \sum_{j=1}^{\infty} \frac{W_{ij}W_{m-i,n+j}}{a^2} \left[j^2 + jn + n^2 + \frac{\pi^2 a^2}{3\ell^2} (-im+i^2+m^2) \right] \Bigg\}$$

$$+ \frac{1}{8} \Bigg\{ \sum_{i=1}^{m-1} \sum_{j=1}^{n-1} \frac{W_{ij}W_{m-i,n-j}}{a^2} \Bigg\langle (nj+j^2) + \frac{\pi^2 a^2}{3\ell^2} (mi+i^2) - \frac{h\bar{n}j}{6a^2} (n-j)(2j-n)$$

$$+ \frac{m\pi^4}{12} \left(\frac{a}{\ell}\right)^2 \left(\frac{h}{a}\right)^2 i(m-i)(m-2i) + \frac{\pi^2}{18} \left(\frac{h}{a}\right)^2 \left(\frac{a}{\ell}\right)^2 [ni(m-i)(n-2j)$$

$$+ mj(n-j)(m-2i)] \Bigg\rangle \Bigg\} = 0 \qquad (4.4)$$

The equations for the other Fourier coefficients are structurally similar to (4.4). For small values of time these equations can be approximated by retaining only those quadratic terms which involve W_{oo} and either U_{mn}, V_{mn} or W_{mn}. The results are

$$\ddot{U}_{mn} + C_1 U_{mn} + C_2 V_{mn} + C_3 W_{mn} = 0 \qquad (4.5a)$$

$$\ddot{V}_{mn} + C_4 V_{mn} + C_2 U_{mn} + C_5 W_{mn} = 0 \qquad (4.5b)$$

$$\ddot{W}_{mn} + C_3 U_{mn} + C_5 V_{mn} + W_{mn} \left\{ C_6 + \frac{W_{oo}}{a} \left[n^2 + \frac{m^2\pi^2}{3} \left(\frac{a}{\ell}\right)^2 \right] \right\} = 0 \qquad (4.5c)$$

where C_1 through C_6 are as defined in (3.3) In Chapter III it was shown that a good approximation to the linear response is obtained by neglecting tangential inertia. Extending this conclusion to the motion considered here yields from (4.5a and (4.5b)

$$U_{mn} = \frac{(C_2C_5 - C_3C_4)}{(C_1C_4 - C_2^2)} W_{mn} \qquad (4.6a)$$

$$V_{mn} = \frac{(C_2C_3-C_1C_5)}{(C_1C_4-C_2^2)} W_{mn} \tag{4.6b}$$

Introducing these together with W_{oo} from (4.3) into (4.5c) gives

$$\ddot{W}_{mn} + (\Omega + \mu \sin \tau)W_{mn} = 0 \tag{4.6c}$$

where

$$\Omega = C_6 \frac{C_5^2}{C_4} + \frac{(C_3C_4-C_2C_5)^2}{C_4(C_2^2-C_1C_4)} \tag{4.6d}$$

$$\mu = \frac{v_o}{c}\left[n^2 + \frac{m^2\pi^2}{3}\left(\frac{a}{\ell}\right)^2\right] \tag{4.6e}$$

Equation (4.6c) is Mathieu's equation, whose properties and solutions are extensively recorded such as in Ref. 6. The character of the solutions is determined by the parameters Ω and μ. Figure 7 shows the Mathieu stability diagram. If a point (Ω,μ) falls within a shaded region, the solution is bounded or stable; if the point falls within an unshaded region, the solution exhibits exponential growth. In the present problem the amplitude of a given mode will remain perturbational in size whenever its corresponding parameter point falls into a stable region. But significant growth may be expected in a mode whose parameter point falls in an unstable region.

The first unstable region, in the vicinity of $\Omega = 1/4$, will be of particular interest since it is "most open" for a reasonable bound on μ. In this zone the values of μ will be practically limited by the shell geometry and initial velocity. While it appears that μ can have an arbitrarily large value in this first region by simply increasing m and n, it should be noted that Ω

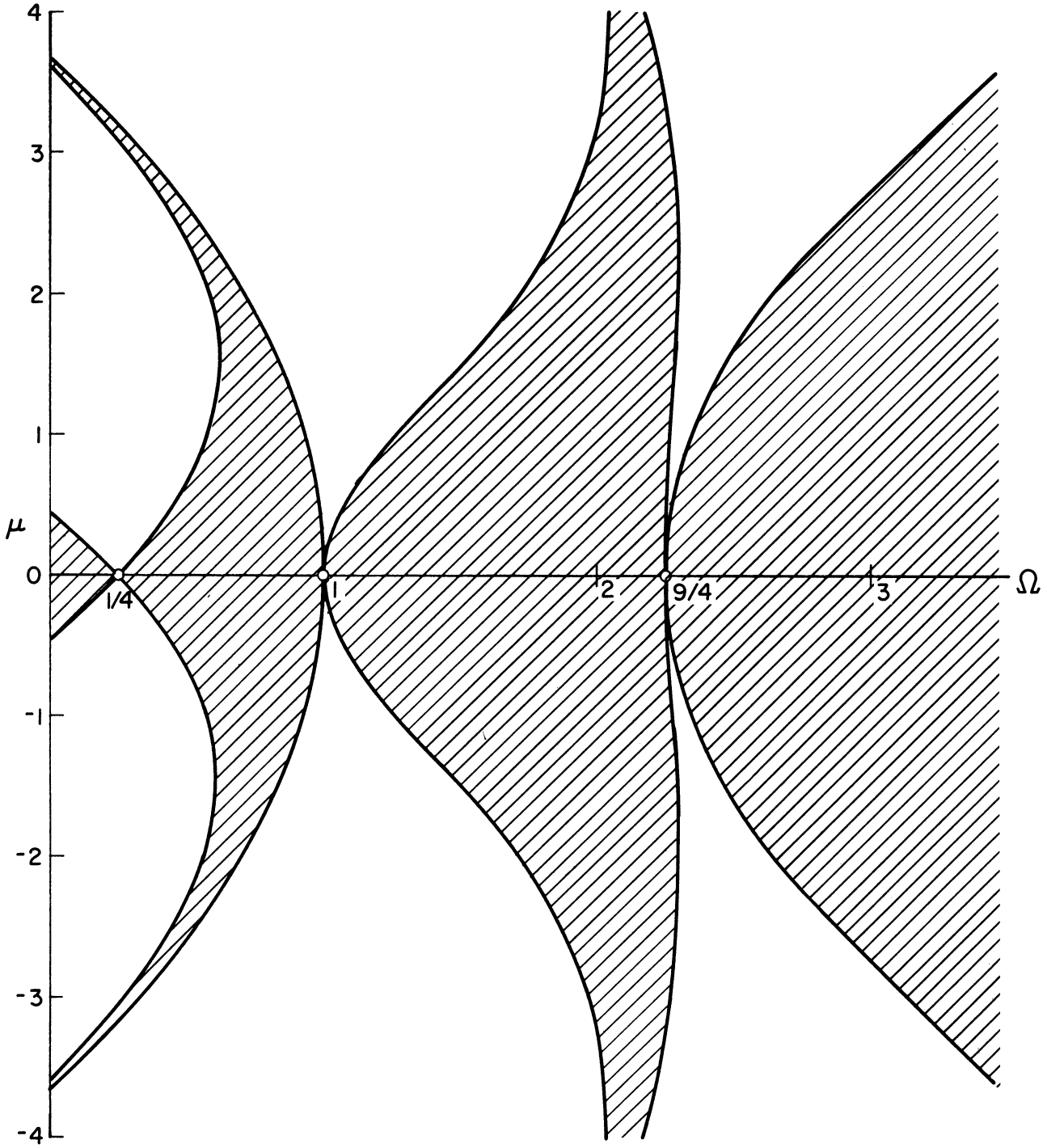

Fig. 7. Mathieu stability diagram.

behaves as (m^4+n^4) for large m and n while μ behaves like (m^2+n^2), i.e., a large value of μ corresponds to a much greater value of Ω.

Generally, in an unshaded zone, the farther a point is from the stable boundary, the faster the solution will grow. For points centrally located in the first and second open regions at equal values of μ, the growth rate for the point in the second region will be negligible compared to that of the first.

The dependence of Ω and μ upon geometry is shown in Figs. 8, 9, and 10. Figure 8 shows data for $(a/\ell) = 1$ and $(a/h) = 100$. If the thickness is increased, fewer points will fall into an unstable region as shown in Fig. 9. If the shell is lengthened, more points move into the first zone from the right which can be seen by comparing Figs. 8 and 10. As the length becomes arbitrarily large, for each n the points for all values of m coalesce to the $m = 0$ point.

In a particular problem, a large number of points may be located in the first unstable region. It is expected that the modes with high growth rates will dominate the response. Thus many of the unstable modes may be neglected based upon a comparison of their growth rates. As will be seen, the accuracy of this approximation can be evaluated in the long term analysis.

The study of the initial response of the shell has allowed the determination of those modes which may be strongly excited. The subsequent behavior of these modes will characterize the finite time response of the shell.

B. LONG TERM ANALYSIS

To obtain solutions to the nonlinear differential equations for the

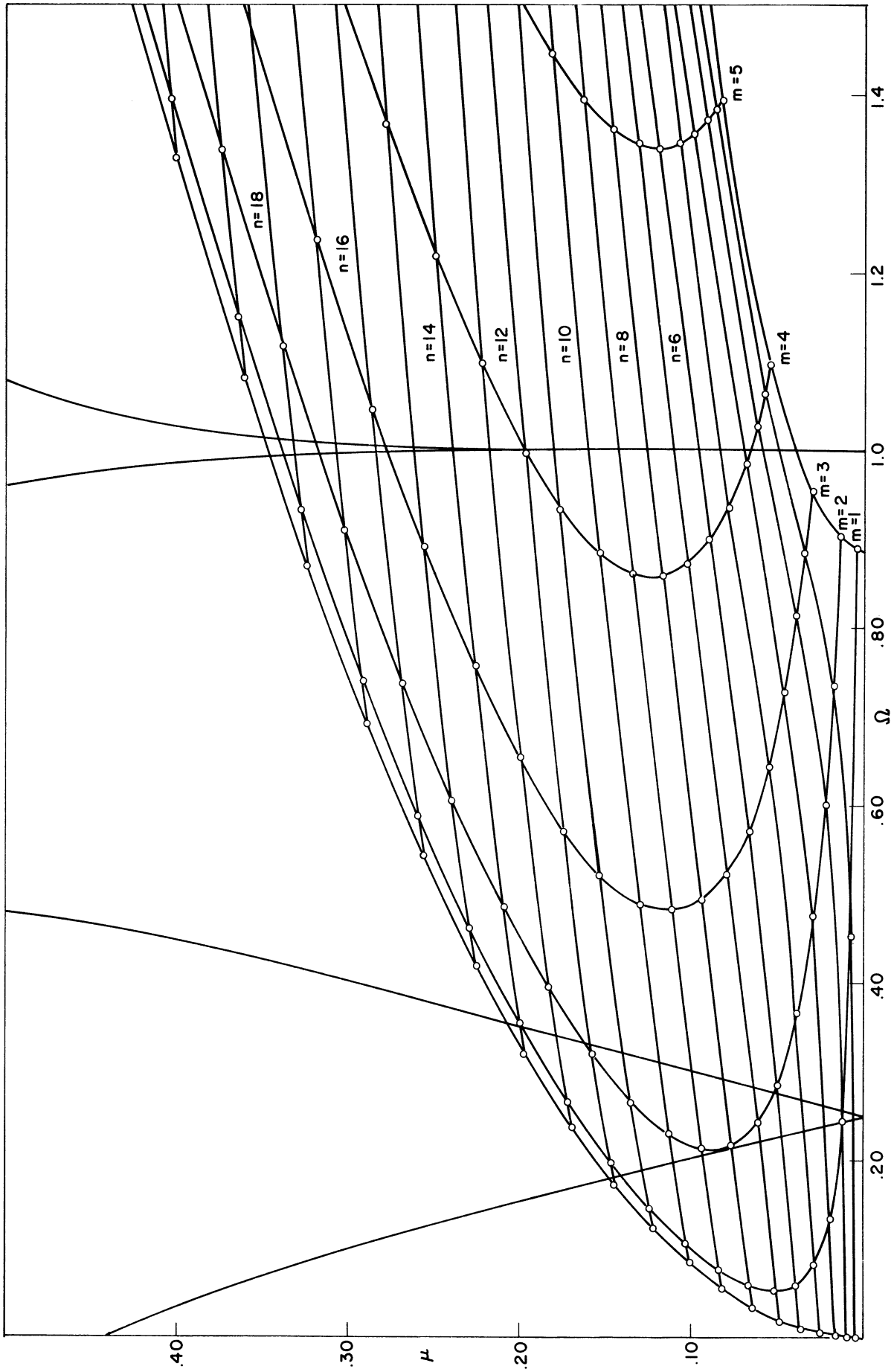

Fig. 8. Stability diagram for $v_o/c = 10^{-3}$, $a/\ell = 1$, $a/h = 100$.

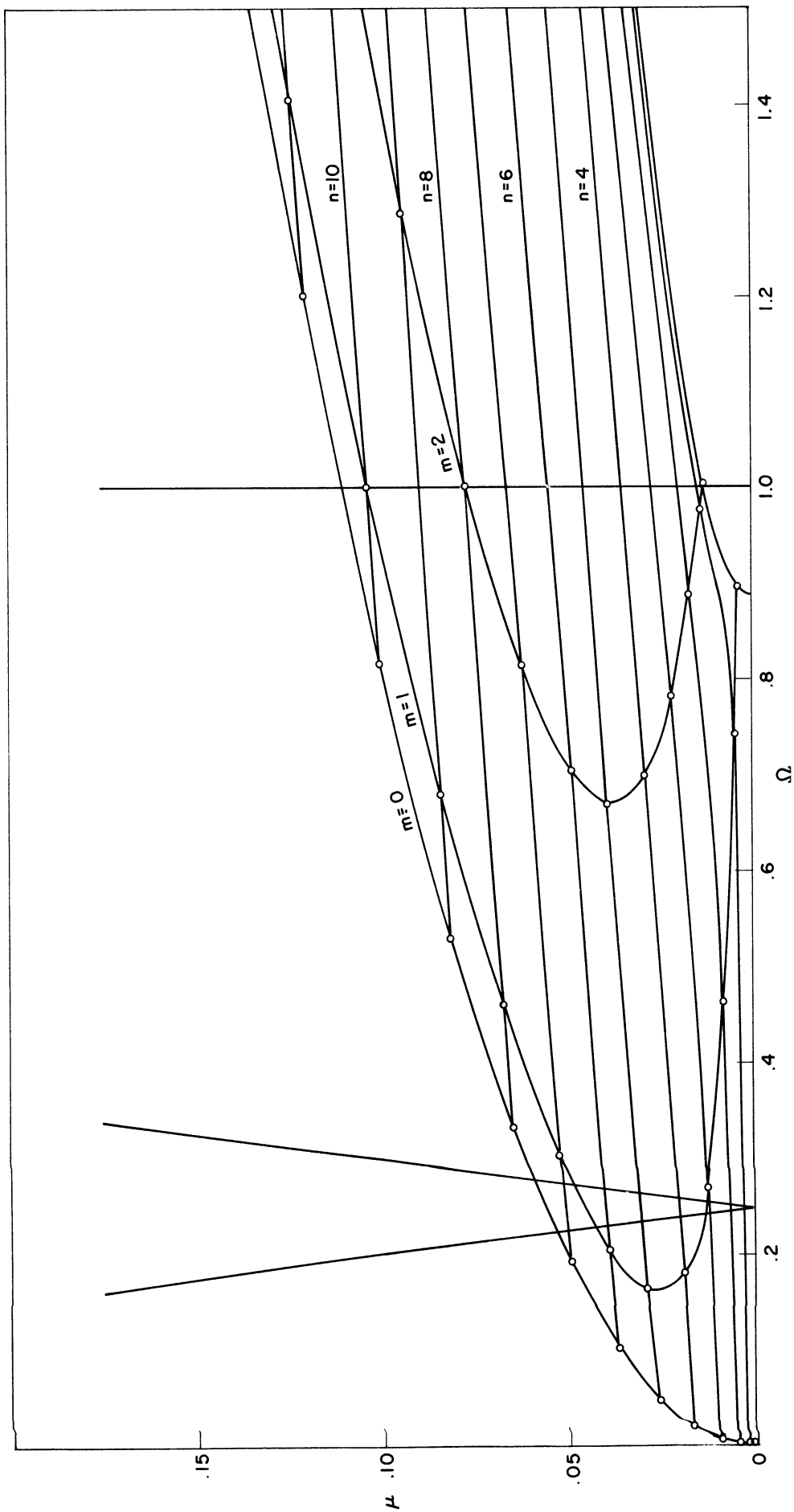

Fig. 9. Stability diagram for $v_o/c = 10^{-3}$, $a/\ell = 1$, $a/h = 31.5$.

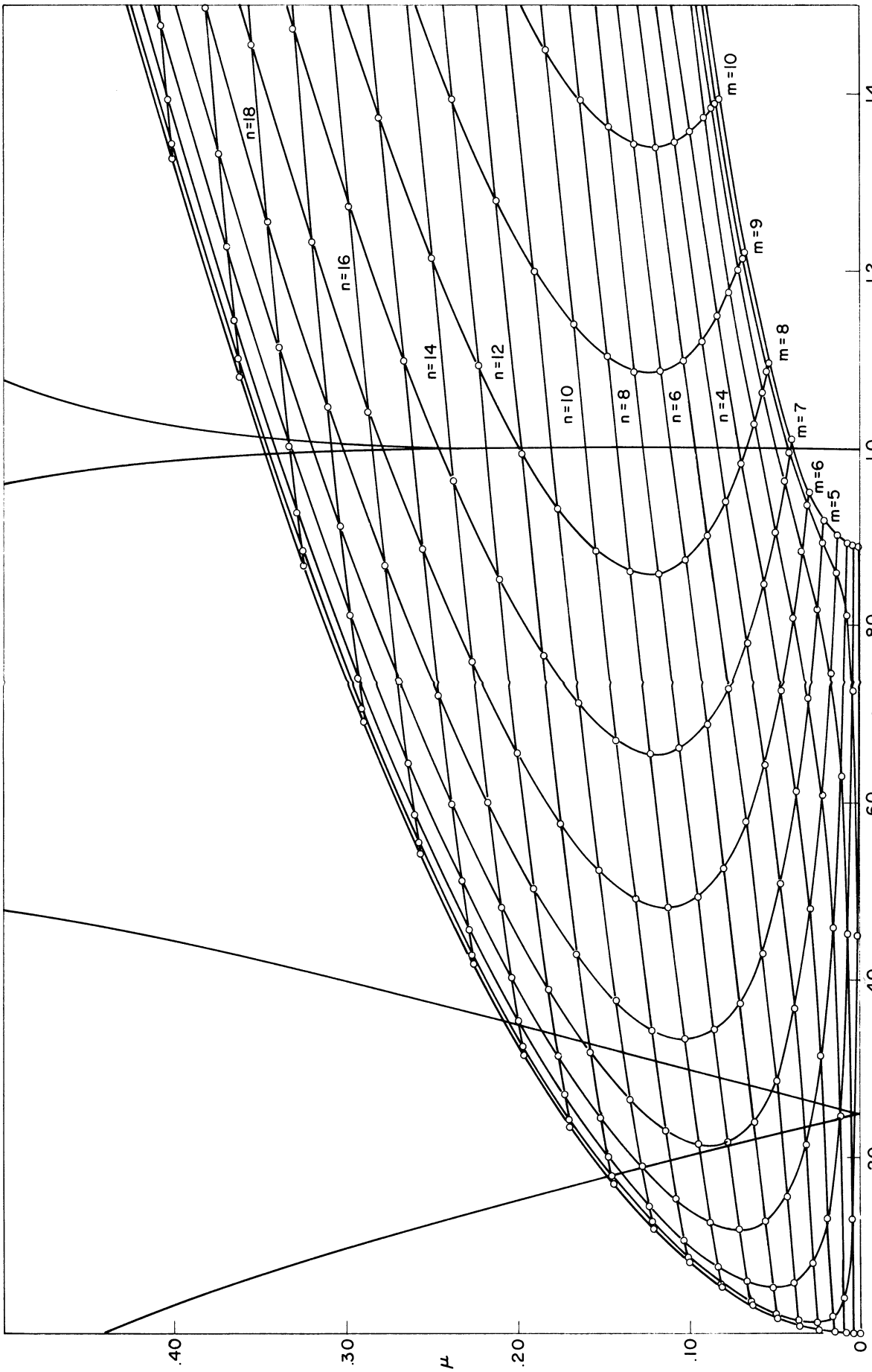

Fig. 10. Stability diagram for $v_o/c = 10^{-3}$, $a/\ell = 1/2$, $a/h = 100$.

Fourier coefficients, it is necessary to consider specific problems. The shell geometry and initial velocity distribution will be prescribed in the examples that follow.

Since not all possible "unstable" modes will be included in the analysis, the accuracy of the solutions will be ascertained by computing the strain energy and kinetic energy of all participating modes and comparing the sum to the kinetic energy initially imparted to the shell. In addition, the energy of the slowest growing of the selected modes should be essentially negligible compared to the initial energy to assure that the excluded modes have an insignificant effect upon the solutions.

1. Example 1

The geometry is prescribed by $(a/\ell) = 1.0$ and $(a/h) = 100$. The stability diagram in the vicinity of $\Omega = 1/4$ is shown in Fig. 11. Ten modes are susceptible to excitation. The initial motion of the perturbed modes is determined from (4.6c). For the modes with parameter points in the unstable zone, the solution is of the form $e^{k\tau}\phi(\tau)$ where $\phi(\tau)$ is periodic. Iso-k curves are shown in the diagram. The four fastest growing modes, (0,13), (1,13), (0,14), and (2.11), are included in the analysis. The governing differential equations are

$$\frac{\ddot{W}_{00}}{a} + \frac{W_{00}}{a} + \frac{1}{4}\left\{(13)^2\frac{W_{0,13}^2}{a^2} + (14)^2\frac{W_{0,14}^2}{a^2} + \frac{W_{1,13}^2}{a^2}\left[\frac{(13)^2}{2} + \frac{\pi^2(1)^2}{6}\left(\frac{a}{\ell}\right)^2\right]\right.$$
$$\left. + \frac{W_{2,11}^2}{a^2}\left[\frac{(11)^2}{2} \quad \frac{\pi^2(2)^2}{6}\left(\frac{a}{\ell}\right)^2\right]\right\} = 0 \qquad (4.7a)$$

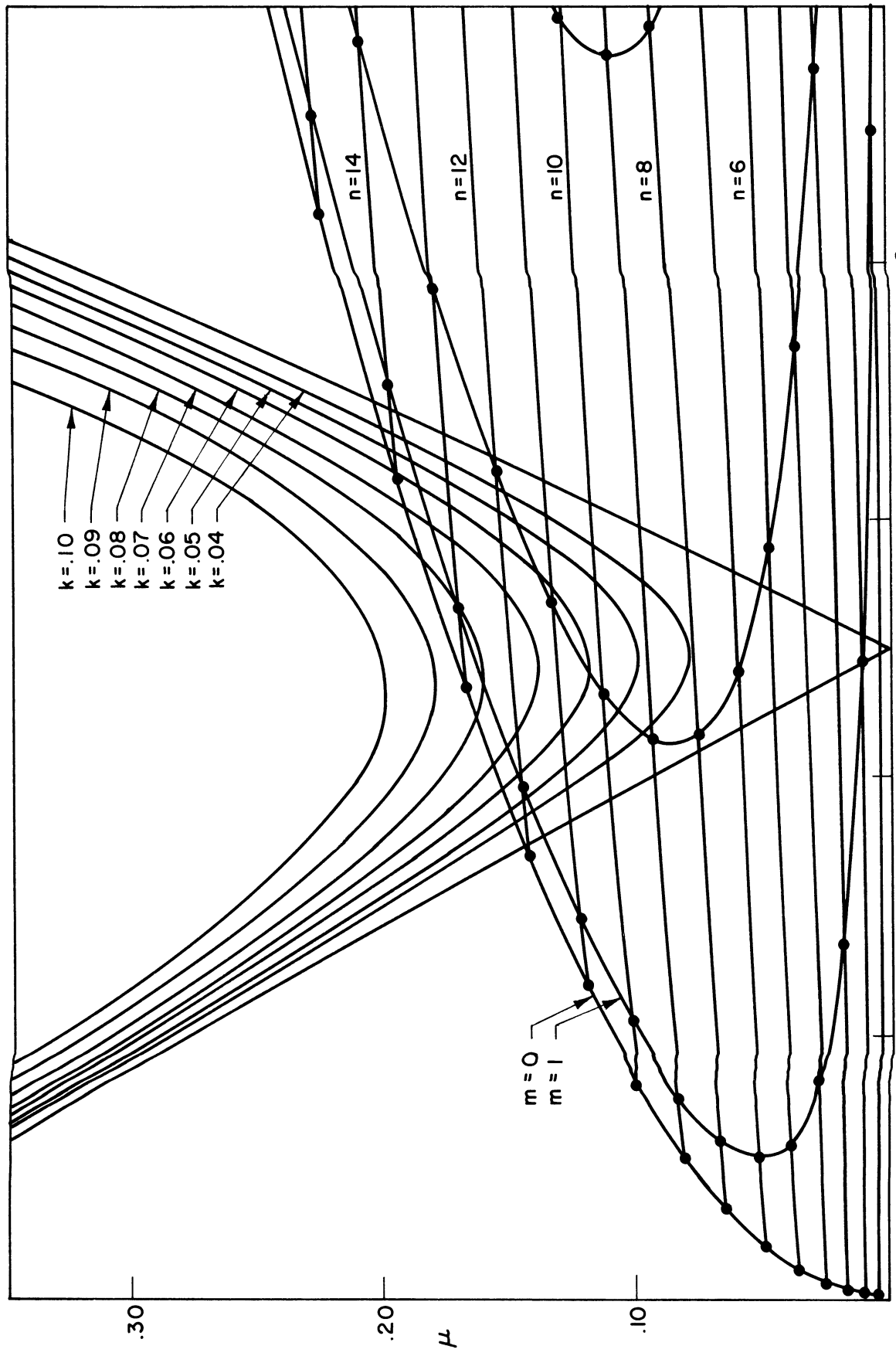

Fig. 11. Stability diagram near $\Omega = 1/4$. $v_o/c = 10^{-3}$, $a/\ell = 1$, $a/h = 100$.

$$\frac{\ddot{W}_{0,13}}{a} + \frac{W_{0,13}}{a}\left\{1 + \frac{h^2}{12a^2}\left[(13)^4 - 2(13)^2\right] + \frac{(13)^2 W_{00}}{a}\right\} + 13V_{0,13} = 0 \tag{4.7b}$$

$$\frac{\ddot{W}_{0,14}}{a} + \frac{W_{0,14}}{a}\left\{1 + \frac{h^2}{12a^2}\left[(14)^4 - 2(14)^2\right] + \frac{(14)^2 W_{00}}{a}\right\} + 14V_{0,14} = 0 \tag{4.7c}$$

$$\frac{\ddot{W}_{1,13}}{a} + \frac{W_{1,13}}{a}\left\{1 + \frac{1}{12}\left(\frac{h}{a}\right)^2\left[(13)^4 - (2)(13)^2 + (1)^4\pi^4\left(\frac{a}{\ell}\right)^4 + \frac{(1)^2(13)^2\pi^2}{6}\left(\frac{a}{\ell}\right)\right]\right\}$$
$$+ \frac{V_{1,13}}{a}\left[13 + \frac{(13)\pi^2(1)^2}{12}\left(\frac{h}{a}\right)^2\left(\frac{a}{\ell}\right)^2\left(1 + \frac{13}{3}\right)\right] + \frac{U_{1,13}}{a}\left(\frac{\pi}{3}\right)\left(\frac{a}{\ell}\right)$$
$$(x)\left\{(1) + \frac{(1)}{4}\left(\frac{h}{a}\right)^2\left[\pi^2(1)^2\left(\frac{a}{\ell}\right)^2 - \frac{(1)(13)^2}{3}\right]\right\}$$
$$+ \frac{W_{00}\,W_{1,13}}{a^2}\left[(13)^2 + \frac{(1)^2\pi^2}{3}\left(\frac{a}{\ell}\right)^2\right] = 0 \tag{4.7d}$$

$$\frac{\ddot{W}_{2,11}}{a} + \frac{W_{2,11}}{a}\left\{1 + \frac{1}{12}\left(\frac{h}{a}\right)^2\left[(11)^4 - (2)(11)^2 + (2)^4\pi^4\left(\frac{a}{\ell}\right)^4 + \frac{(2)^2(11)^2\pi^2}{6}\left(\frac{a}{\ell}\right)^2\right]\right\}$$
$$+ \frac{V_{2,11}}{a}\left[11 + \frac{(11)\pi^2(2)^2}{12}\left(\frac{h}{a}\right)^2\left(\frac{a}{\ell}\right)^2\left(1 + \frac{11}{3}\right)\right]$$
$$+ \frac{U_{2,11}}{a}\left(\frac{\pi}{3}\right)\left(\frac{a}{\ell}\right)\left\{(2) + \frac{(2)}{4}\left(\frac{h}{a}\right)^2\left[\pi^2(2)^2\left(\frac{a}{\ell}\right)^2 - \frac{(2)(11)^2}{3}\right]\right\}$$
$$+ \frac{W_{00}W_{2,11}}{a^2}\left[(11)^2 + \frac{(2)^2\pi^2}{3}\left(\frac{a}{\ell}\right)^2\right] = 0 \tag{4.7e}$$

Equations (4.6a) and (4.6b) are used to express U_{mn} and V_{mn} in terms of W_{mn}.

In this example, the initial conditions selected are

$$\frac{\dot{W}_{00}(o)}{a} = \frac{v_o}{c} \tag{4.8a}$$

$$\frac{\dot{W}_{mn}(o)}{a} = \frac{v_o}{c}\frac{\Delta}{(m^2+n^2)} \qquad m,n > 0 \tag{4.8b}$$

in which $v_o/c \ll 1$, $\Delta \ll 1$.

The Fourier coefficients obtained from the numerical integration of (4.7) using (4.8) are shown in Fig. 12. The response is characterized by a cyclic exchange of energy between the various modes. The largest amplitude is reached by mode (1,13); this is also the first mode to reach its maximum value.

The ratio of the total energy in each mode to the original kinetic energy of the shell was computed and is shown in Fig. 13. The mode with the slowest growth rate, (2,11), participates with almost negligible energy during the initial exchanges and never contains more than 15% of the total energy for the values of time considered. The maximum difference between the sum of the energies in the participating modes and the original kinetic energy does not exceed one half of 1% in this example.

2. Example 2

Here a second perturbation is considered with the same geometry as in Example 1. The initial radial velocity distribution is assumed to be a constant perturbed by a parabolic variation expressed as

$$\frac{\dot{w}}{a}(x,\theta,o) = \frac{v_o}{c}\left[1 + \Delta\left(\frac{x}{\ell}\right)^2\left(1 - \frac{4\theta^2}{\pi^2}\right)\right], \quad -\frac{\pi}{2} \le \theta \le \frac{\pi}{2}$$

$$= \frac{v_o}{c}, \qquad \frac{\pi}{2} \le \theta \le \frac{3\pi}{2} \qquad (4.9)$$

in which $v_o/c \ll 1$, $\Delta \ll 1$.

The initial values of the coefficients are

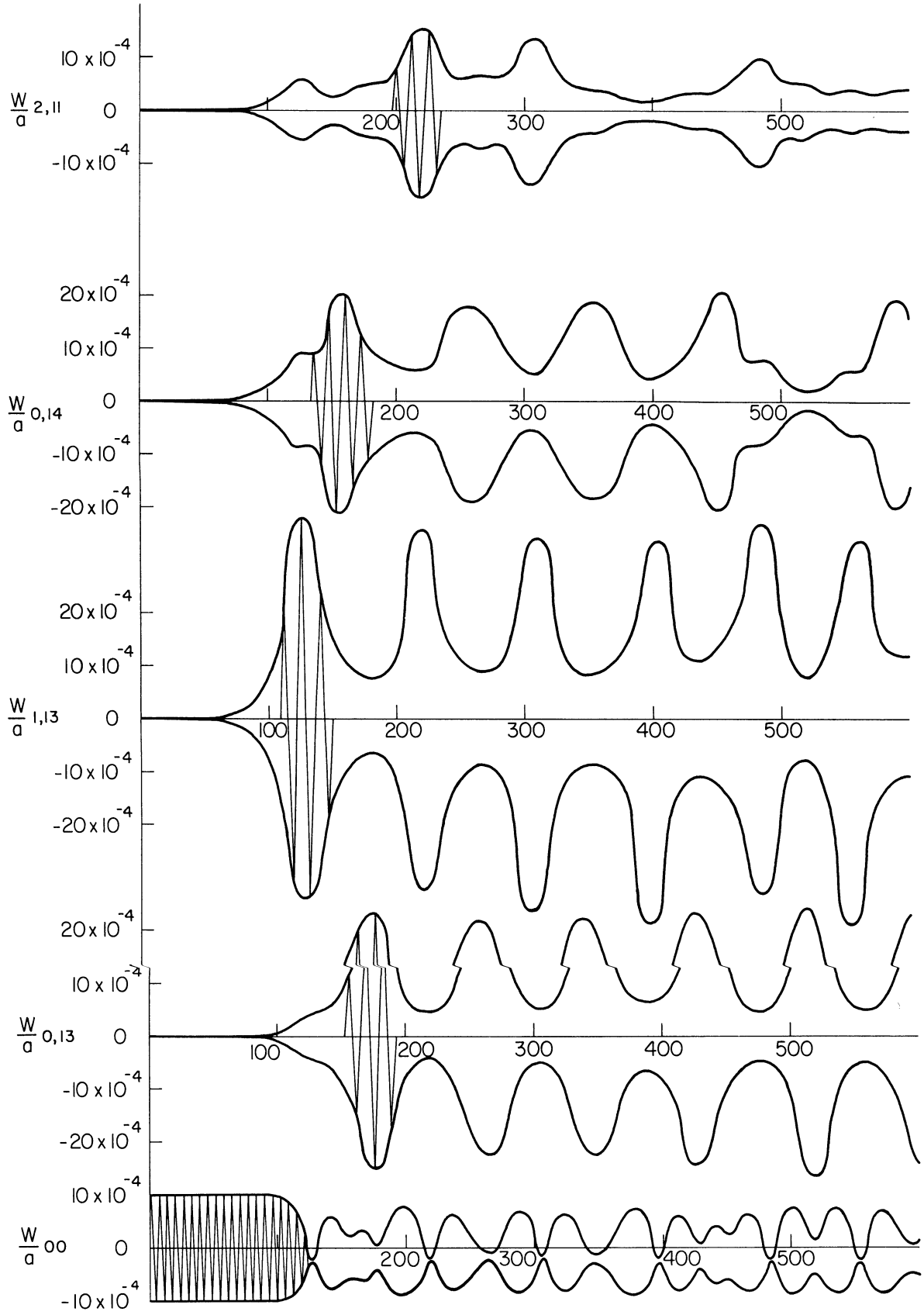

Fig. 12. Displacement coefficients vs. time. $v_o/c = 10^{-3}$, $a/\ell = 1$, $a/h = 100$, $\epsilon_{mn} = 1/(m^2+n^2)$.

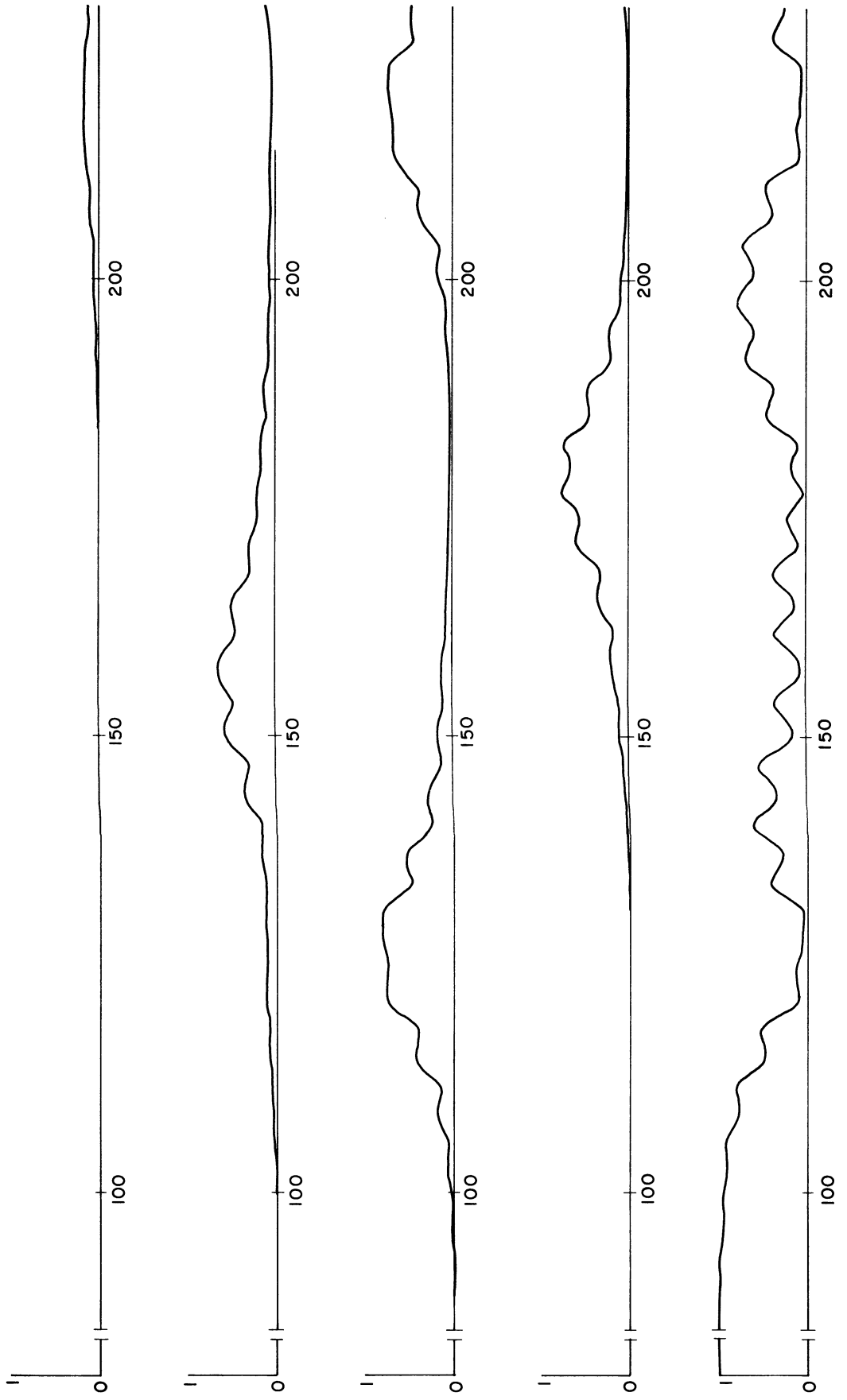

Fig. 13. Ratio of energy in each mode to initial kinetic energy vs. time. $v_o/c = 10^{-3}$, $a/\ell = 1$, $a/h = 100$, $\epsilon_{mn} = 1/(m^2+n^2)$.

$$\frac{\dot{W}_{mn}(o)}{a} = \frac{32v_o\Delta(-1)^m}{c\pi^4m^2n^2}\left(\frac{2}{n\pi}\sin\frac{n\pi}{2} - \cos\frac{n\pi}{2}\right), \quad m,n > 0 \qquad (4.10a)$$

$$\frac{\dot{W}_{on}(o)}{a} = \frac{8v_o\Delta}{3c\pi^2n^2}\left(\frac{2}{n\pi}\sin\frac{n\pi}{2} - \cos\frac{n\pi}{2}\right), \quad n > 0 \qquad (4.10b)$$

$$\frac{\dot{W}_{oo}(o)}{a} = \frac{v_o}{c}\left(1 + \frac{\Delta}{9}\right) \doteq \frac{v_o}{c} \qquad (4.10c)$$

The differential equations (4.7) have been integrated numerically with these initial conditions. The solutions for the displacement coefficients are displayed in Fig. 14. Although the coefficient for mode (0,14) reaches its maximum magnitude first, the largest amplitude is attained by (1,13) a few cycles later when essentially all of the energy in the fundamental mode has been extracted.

In comparing the results of the two examples, the fact that mode (0,14) reaches its maximum value first in the second example can be attributed to the relative size of the perturbations. In Example 1 the perturbations received by each mode were of comparable magnitude, while in Example 2 the initial velocity for mode (0,14) was approximately 15 times as strong as that for mode (1,13). The maximum amplitudes of these modes are rather insensitive to changes in the perturbation.

3. Example 3

The geometry is modified by specifying $(a/\ell) = 1/2$ and $(a/h) = 100$. The Mathieu stability diagram in the vicinity of $\Omega = 1/4$ is shown in Fig. 15. Of the 16 modes that may be classified as unstable, the six modes assumed to dominate the motion are (0,13), (1,13), (2,13), (3,12), (4,11), and (0,14).

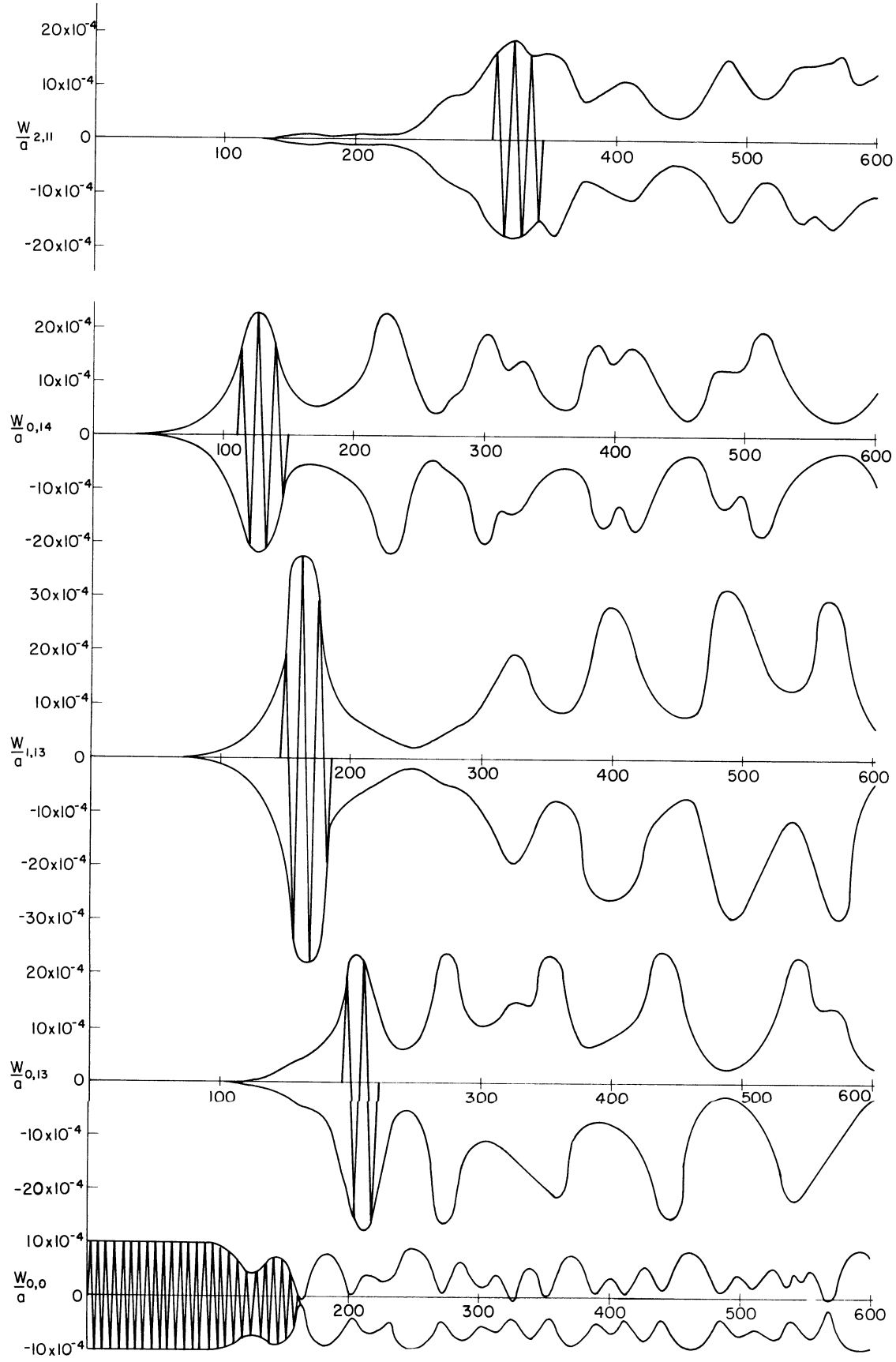

Fig. 14. Displacement coefficients vs. time for the parabolic perturbation. $v_o/c = 10^{-3}$, $a/\ell = 1$, $a/h = 100$.

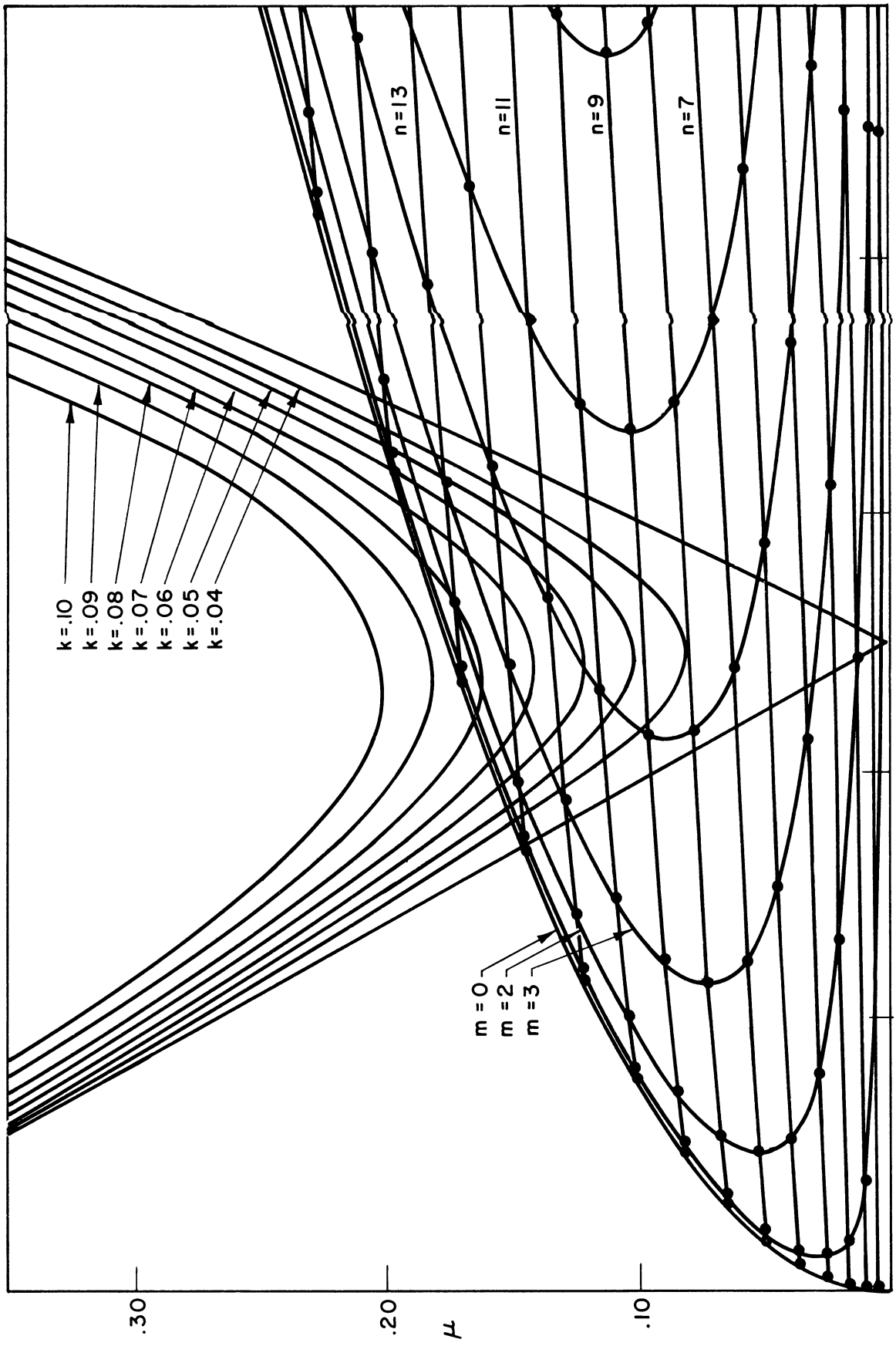

Fig. 15. Stability diagram near $\Omega = 1/4$. $v_o/c = 10^{-3}$, $a/\ell = 1/2$, $a/h = 100$.

The differential equations for the Fourier coefficients are

$$\frac{\ddot{W}_{00}}{a} + \frac{W_{00}}{a} + \frac{1}{4}\left\{(13)^2\,\frac{W_{0,13}^2}{a} + (14)^2\,\frac{W_{0,14}^2}{a^2} + \frac{W_{1,13}^2}{a^2}\left[\frac{(13)^2}{2} + \frac{\pi^2(1)^2}{6}\left(\frac{a}{\ell}\right)^2\right]\right.$$
$$+ \frac{W_{2,13}^2}{a^2}\left[\frac{(13)^2}{2} + \frac{\pi^2(2)^2}{6}\left(\frac{a}{\ell}\right)^2\right] + \frac{W_{3,12}^2}{a^2}\left[\frac{(12)^2}{2} + \frac{\pi^2(3)^2}{6}\left(\frac{a}{\ell}\right)^2\right]$$
$$\left. + \frac{W_{4,11}^2}{a^2}\left[\frac{(11)^2}{2} + \frac{\pi^2(4)^2}{6}\left(\frac{a}{\ell}\right)^2\right]\right\} = 0 \qquad (4.11a)$$

$$\frac{\ddot{W}_{0,13}}{a} + \frac{W_{0,13}}{a}\left\{1 + \frac{h^2}{12a^2}\left[(13)^4 - 2(13)^2\right] + (13)^2\,\frac{W_{00}}{a}\right\} + 13V_{0,13} = 0 \qquad (4.11b)$$

$$\frac{\ddot{W}_{0,14}}{a} + \frac{W_{0,14}}{a}\left\{1 + \frac{h^2}{12a^2}\left[(14)^4 - 2(14)^2\right] + (14)^2\,\frac{W_{00}}{a}\right\} + 14V_{0,14} = 0 \qquad (4.11c)$$

$$\frac{\ddot{W}_{1,13}}{a} + \frac{W_{1,13}}{a}\left\{1 + \frac{h^2}{12a^2}\left[(13)^2 - (2)(13)^2 + (1)^4\pi^4\left(\frac{a}{\ell}\right)^4 + \frac{(1)^2(13)^2\pi^2}{6}\left(\frac{a}{\ell}\right)^2\right]\right\}$$
$$+ \frac{V_{1,13}}{a}\left[13 + \frac{(13)\pi^2(1)^2}{12}\left(\frac{h}{a}\right)^2\left(\frac{a}{\ell}\right)^2\left(1 + \frac{13}{3}\right)\right]$$
$$+ \frac{U_{1,13}}{a}\left(\frac{\pi}{3}\right)\left(\frac{a}{\ell}\right)\left\{(1) + \frac{1}{4}\left(\frac{h}{a}\right)^2\left[\pi^2(1)^2\left(\frac{a}{\ell}\right)^2 - \frac{(1)(13)^2}{3}\right]\right\}$$
$$+ \frac{W_{00}W_{1,13}}{a^2}\left[(13)^2 + \frac{(1)^2\pi^2}{3}\left(\frac{a}{\ell}\right)^2\right] = 0 \qquad (4.11d)$$

$$\frac{\ddot{W}_{2,13}}{a} + \frac{W_{2,13}}{a}\left\{1 + \frac{1}{12}\left(\frac{h}{a}\right)^2\left[(13)^2 - 2(13)^2 + (2)^4\pi^4\left(\frac{a}{\ell}\right)^4 + \frac{(2)^2(13)^2\pi^2}{6}\left(\frac{a}{\ell}\right)^2\right]\right\}$$
$$+ \frac{V_{2,13}}{a}\left[13 + (13)\,\frac{\pi^2(2)^2}{12}\left(\frac{h}{a}\right)^2\left(\frac{a}{\ell}\right)^2\left(1 + \frac{13}{3}\right)\right.$$
$$+ \frac{U_{2,11}}{a}\left(\frac{\pi}{3}\right)\left(\frac{a}{\ell}\right)\left\{(2) + \frac{(2)}{4}\left(\frac{h}{a}\right)^2\left[\pi^2(2)^2\left(\frac{a}{\ell}\right)^2 - \frac{(2)(13)^2}{3}\right]\right\}$$
$$+ \frac{W_{00}W_{2,13}}{a^2}\left[(13)^2 + \frac{(2)^2\pi^2}{3}\left(\frac{a}{\ell}\right)^2\right] = 0 \qquad (4.11e)$$

$$\frac{\ddot{W}_{3,12}}{a} + \frac{W_{3,12}}{a}\left\{1 + \frac{h^2}{12a^2}\left[(12)^2 - 2(12)^2 + (3)^4\pi^4\left(\frac{a}{\ell}\right)^4 + \frac{(3)^2(12)^2\pi^2}{6}\left(\frac{a}{\ell}\right)^2\right]\right\}$$

$$+ \frac{V_{3,12}}{a}\left[12 + \frac{(12)\pi^2(3)^2}{12}\left(\frac{h}{a}\right)^2\left(\frac{a}{\ell}\right)^2\left(1 + \frac{12}{3}\right)\right]$$

$$+ \frac{U_{3,12}}{a}\left(\frac{\pi}{3}\right)\left(\frac{a}{\ell}\right)\left\{(3) + \frac{(3)}{4}\left(\frac{h}{a}\right)^2\left[\pi(3)^2\left(\frac{a}{\ell}\right)^2 - (3)\frac{(12)^2}{3}\right]\right\}$$

$$+ \frac{W_{00}W_{3,12}}{a^2}\left[(12)^2 + \frac{(3)^2\pi^2}{3}\left(\frac{a}{\ell}\right)^2\right] = 0 \qquad (4.11f)$$

$$\frac{\ddot{W}_{4,11}}{a} + \frac{W_{4,11}}{a}\left\{1 + \frac{1}{12}\left(\frac{h}{a}\right)^2\left[(11)^4 + (4)(11)^2 + (4)^4\pi^4\left(\frac{a}{\ell}\right)^4 + (4)^2(11)^2\frac{\pi^2}{6}\left(\frac{a}{\ell}\right)^2\right]\right\}$$

$$+ \frac{V_{4,11}}{a}\left[11 + \frac{(11)\pi^2(4)^2}{12}\left(\frac{h}{a}\right)^2\left(\frac{a}{\ell}\right)^2\left(1 + \frac{11}{3}\right)\right]$$

$$+ \frac{U_{4,11}}{a}\left(\frac{\pi}{3}\right)\left(\frac{a}{\ell}\right)\left\{(4) + \frac{(4)}{4}\left(\frac{h}{a}\right)^2\left[\pi^2 4^2\left(\frac{a}{\ell}\right)^2 - \frac{(4)(11)^2}{3}\right]\right\}$$

$$+ \frac{W_{00}W_{4,11}}{a^2}\left[(11)^2 + \frac{(4)^2\pi^2}{3}\left(\frac{a}{\ell}\right)^2\right] = 0 \qquad (4.11g)$$

For this problem the initial conditions will be the same as for Example 2, that is

$$\frac{\dot{W}}{a}(x,\theta,o) = \frac{v_o}{c}\left[1 + \Delta\left(\frac{x}{\ell}\right)^2\left(1 - \frac{4\theta^2}{\pi^2}\right)\right], \quad -\frac{\pi}{2} \le \theta \le \frac{\pi}{2}$$

$$= \frac{v_o}{c}, \qquad \frac{\pi}{2} \le \theta \le \frac{3\pi}{2} \qquad (4.12)$$

The solutions for the displacement coefficients are shown in Fig. 16. The response is dominated by modes (0,13), (1,13), and (0,14). The amplitudes of modes (2,13), (3,12), and (4,11) are in fact too small to record on the diagram. For example, the ratio of the maximum amplitude of the coefficient of mode (3,12) to that of mode (1,13) is approximately 1.5×10^{-4}. The fact

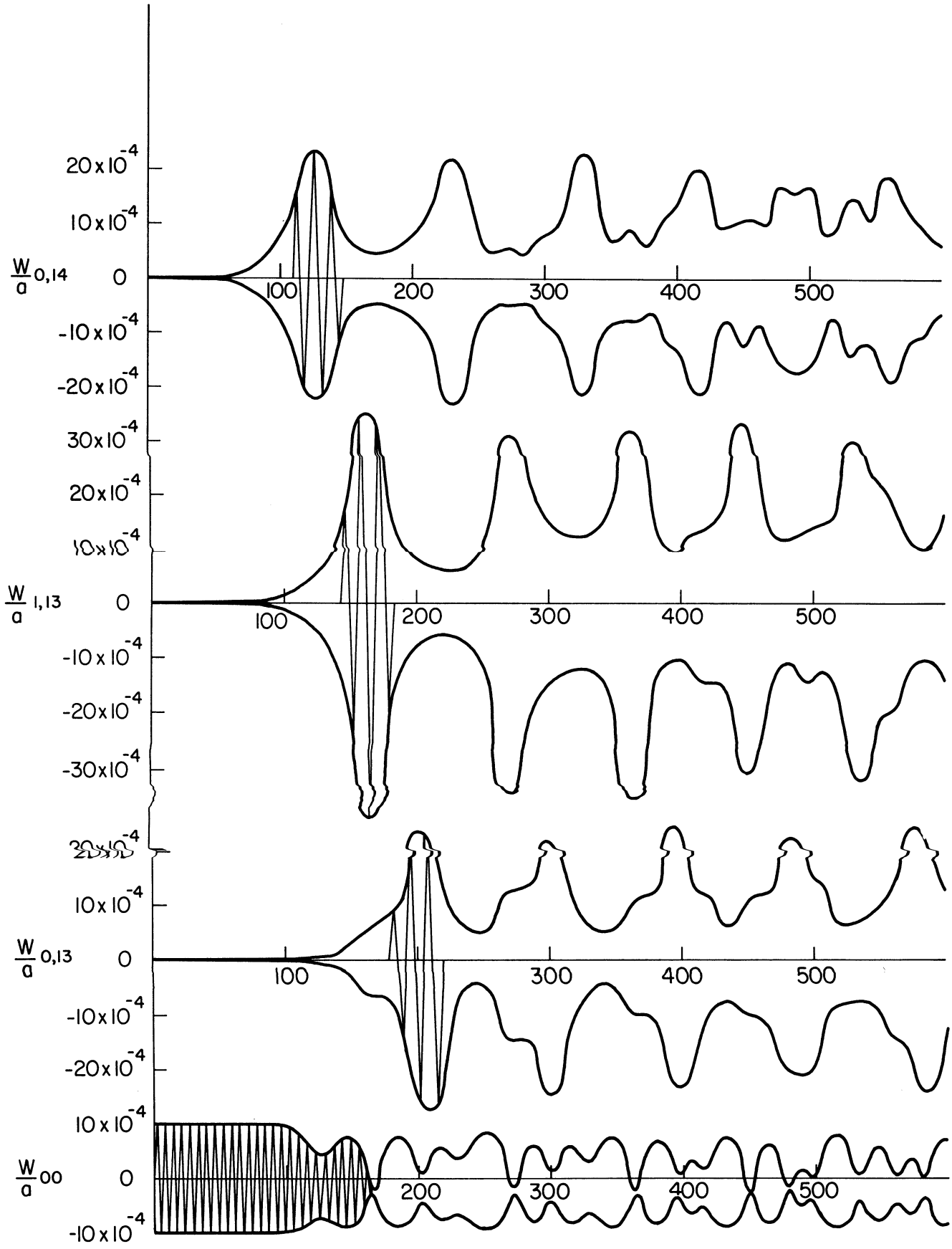

Fig. 16. Displacement coefficients vs. time for the parabolic perturbation. $v_o/c = 10^{-3}$, $a/\ell = 1/2$, $a/h = 100$.

that the perturbation magnitude is not an important issue for the slow growth modes can be emphasized in this case by noting that the coefficient for mode (3,12) received an initial velocity 10 times as large as (1,13).

The shell used in Example 3 was twice as long as that of Example 2 while the velocity perturbations were the same for each case. Although a greater number of flexural modes were classified as initially unstable for the longer shell, the long term response was essentially dominated by the same three flexural modes in both examples.

4. Axial and Circumferential Normal Stress

The large displacements which develop in the finite time response of the shell are accompanied by comparably magnified stresses. In many applications, the stress level would be of prime importance.

For a state of plane stress the normal stress in the circumferential direction is

$$\sigma_\theta = \frac{E}{(1-\nu^2)}\left[\nu\bar{u}_x + \frac{\bar{v}_\theta}{a} + \frac{\bar{w}}{a} - \frac{z}{a}\left(\bar{w} + a\nu\bar{w}_{xx} + \frac{\bar{w}_{\theta\theta}}{a}\right)\right]$$

$$= \frac{E}{(1-\nu^2)}\sum_{i=0}^{\infty}\sum_{j=0}^{\infty}\left\{\frac{W_{ij}}{a}\left[1 - \frac{z}{a}\left(1-j^2-i^2\nu\,\frac{\pi^2a^2}{\ell^2}\right)\right]\right.$$

$$\left. + j\,\frac{V_{ij}}{a} + i\nu\pi\left(\frac{a}{\ell}\right)\frac{U_{ij}}{a}\right\}\cos\frac{i\pi x}{\ell}\cos j\theta\ . \qquad (4.13a)$$

The axial stress is

$$\sigma_x = \frac{E}{(1-\nu^2)}\left[\bar{u}_x + \frac{\nu\bar{v}_\theta}{a} + \frac{\nu\bar{w}}{a} - \frac{z}{a}\left(\frac{\nu\bar{w}}{a} + a\bar{w}_{xx} + \frac{\nu\bar{w}_{\theta\theta}}{a}\right)\right]$$

$$= \frac{E}{(1-\nu^2)}\sum_{i=0}^{\infty}\sum_{j=0}^{\infty}\left\{\frac{W_{ij}}{a}\left[\nu - \frac{z}{a}\left(\nu-\nu j^2-i^2\,\frac{\pi^2a^2}{\ell^2}\right)\right]\right.$$

$$\left. + i\pi\left(\frac{a}{\ell}\right)\frac{U_{ij}}{a} + j\nu\,\frac{V_{ij}}{a}\right\}\cos\frac{i\pi x}{\ell}\cos j\theta\ . \qquad (4.13b)$$

For the unperturbed or fundamental motion of the shell, the circumferential stress at the outer surface is

$$\sigma_\theta = \frac{E}{(1-\nu^2)} \frac{W_{oo}}{a} \left(1 - \frac{h}{2a}\right) \tag{4.14}$$

and the maximum value of this function is

$$\sigma_\theta^* = \frac{E}{(1-\nu^2)} \frac{v_o}{c} \left(1 - \frac{h}{2a}\right) \tag{4.15a}$$

The amplitude of the axial stress for the fundamental motion is

$$\sigma_x^* = \frac{E\nu v_o}{(1-\nu^2)c} \left(1 - \frac{h}{2a}\right) \tag{4.15b}$$

The circumferential and axial stresses at a typical point, $x = 0$, $\theta = 0$, $z = h/2$, are computed for Example 2($a/\ell = 1$, $a/h = 100$, $\nu = 1/3$). Equations (4.13) are written as finite sums for the fundamental mode (0,0) and the excited modes (0,13), (1,13), (0,14), and (2,11). The ratios of these stresses to the maximum values obtained from the fundamental motion, (4.15) are shown in Fig. 17. In this example the circumferential and longitudinal stress ratios reach extreme values of 5 and 10, respectively.

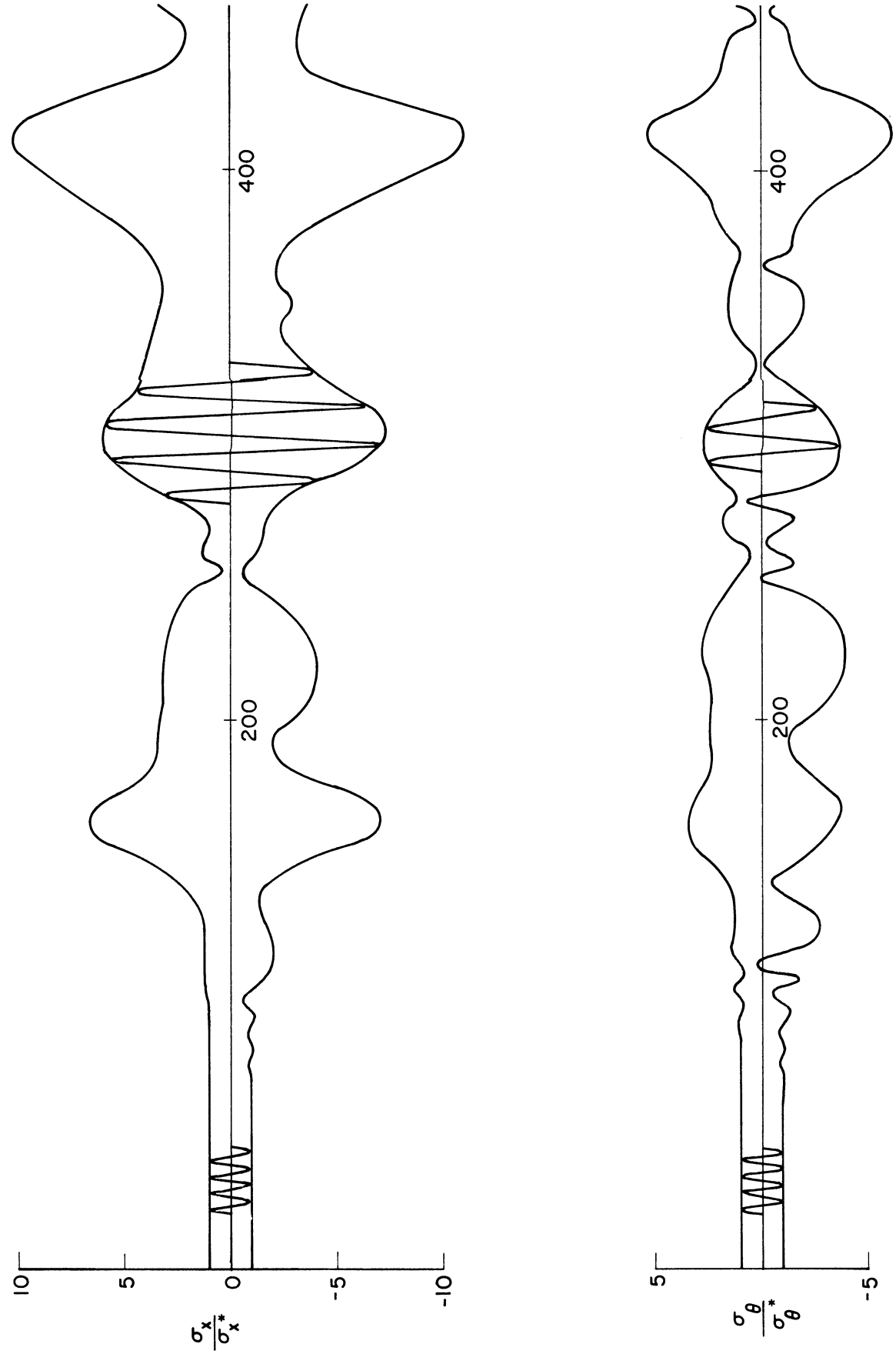

Fig. 17. Stress ratios vs. time for the parabolic perturbation.
$v_o/c = 10^{-3}$, $a/\ell = 1$, $a/h = 100$.

CHAPTER V

CONCLUSIONS

The stability of the motion resulting from the application of a uniform radial impulse to a finite-length cylindrical shell has been analyzed. It has been shown that an unstable response is characterized by the excitation of flexural modes which exchange energy with the basic motion in a cyclic manner. A criterion has been established for the identification of the strongly excited modes. The possibility for such a response is increased both by lengthening the shell and decreasing its thickness.

The growth rates of the perturbed modes can be determined from a short term analysis. Generally the long term behavior is dominated by a few flexural modes having the highest growth rates. The motion is sensitive to changes in the initial perturbations received by these high growth rate modes but is insensitive to changes in the initial values of the slow growth modes. The flexural mode which initially exchanges energy with the basic motion can be changed by modifying the initial perturbation. The maximum amplitudes of the high growth rate modes are essentially unaffected by variations in the magnitudes of the velocity perturbations.

Finally it has been shown that if flexural motion is excited, it gives rise to stresses that are far in excess of those associated with the basic motion of the shell.

BIBLIOGRAPHY

1. Bolotin, V. V., The Dynamic Stability of Elastic Systems, Holden-Day, Inc., San Francisco (1964), pp. 422-426.

2. Goodier, J. N. and McIvor, I. K., "The Elastic Cylindrical Shell Under Nearly Uniform Radial Impulse," J. Appl. Mech. 31, 259-266, 1964.

3. Bieniek, M. P., Fan, T. C., and Lackman, L. M., "Dynamic Stability of Cylindrical Shells," AIAA J. 4, No. 3, 495-500, 1966.

4. Arnold, R. N. and Warburton, G. C., "Flexural Vibrations of the Walls of Thin Cylindrical Shells Having Freely Supported Ends," Proceedings of the Royal Social (London), Series A, 197, 238-256, 1949.

5. Reissner, E., "On Transverse Vibrations of Thin, Shallow Elastic Shells," Quarterly of Appl. Math. 13, No. 2, 169-176, 1955.

6. McLachlan, N. W., Theory and Applications of Mathieu Functions, Dover Publications, Inc., New York (1964).